1 W Physics Program at RHIC

1.1 Questions raised to the W spin physics program

Several questions were raised toward the feasibility and experimental readiness of the W spin physics program. Before going into further detail the different points will be addressed here.

- Can the luminosity needed for a W production program with impact on the antiquark polarizations be achieved?
  For a successful W program to achieve sensitivities to the sea quark polarizations a luminosity of at least 300 pb^{-1} has to be accumulated at an invariant mass $\sqrt{s}$ =500 GeV with a beam polarization of 70%. According to the expected luminosities of the RHIC running in the next years this can be acchieved. It is further discussed in Section 2 of the main spin plan.

- Which detector upgrades are critical for the W program? DOE has ended up confused, for example, about how strong a role the PHENIX FVTX and NCC upgrades are for this program.
  The detector upgrades needed for the W program are the Forward Gem Tracker upgrade (FGT) in STAR and the muon trigger upgrade (consisting of a front end electronics upgrade of the existing tracker and the installation of resistive plate counters (RPC)) in PHENIX. The rejection power of these upgrades alone will be sufficient to detect the W signal and separate it from the background. Further upgrades will improve the extraction of the signal but are not required.

- Can adequate hadronic background suppression be attained in realistic simulations of detector performance, in the absence of a conventional missing energy determination?
  Both experiments have run detailed simulations for detecting Ws in the forward/backward regions which show that the expected backgrounds are understood and that they can be reduced enough to extract the W asymmetries from the data. The background suppression in STAR is at least two orders of magnitude, the hadronic background in PHENIX can be reduced with tight cuts and an additional absorber to obtain a signal to background ratio of 3. Further details, including also mid-rapidity detection and backround, are described below.

- Is present or projected tracking resolution sufficient for adequate charge sign discrimination?
  The tracking resolution and charge sign discrimination capabilities in the barrel part of the STAR detector and the Central arms of the PHENIX detector are already sufficient with one caveat. For STAR studies of potential TPC space charge distortions at

high luminosity have not been completed as of now and present estimates use a factor of 100 in electron-hadron separation. In the forward regions the FGT will allow a charge detection efficiency of more than 90% at 30 GeV. The PHENIX muon arms can distinguish the charge sign with more than 97% efficiency for muon momenta of around 40 GeV.

- What are the respective roles of detector performance and of kinematic ambiguities in limiting x resolution? How will sea antiquark polarizations be extracted from RHIC measurements of W production?
  A determination of x_{Bj} is generally only possible at leading order after knowing the W momentum. In the inclusive measurement the decay smears out such a distinction, however one is still predominantly sensitive to certain regions in x_{Bj} depending on the lepton rapidity and transverse momentum. As the quark polarizations are reasonably known, the differences in the asymmetries can be directly attributed to the sea polarizations in rapidity regions where the sea contribution is large. Similar to the ΔG analysis at RHIC NLO χ^2 distributions can be directly extracted for the sea polarizations and the framework for a global analysis is existing.

- Within projected funding profiles, can we meet the 2013 performance milestone? What are the critical milestones in a plan to get there?
  Three milestones can be identified to ensure a successful W program at RHIC to fulfill the 2013 performance milestone:

  1. Both experiments are ready for mid-rapidity W measurements now. PHENIX will be ready with necessary trigger upgrades for the 2010 run, for the forward/backward muons. STAR will be ready for faroward/backward electrons for the 2011 run following the present plan.
  2. The luminosities needed for the determination of the sea quark polarizations are high - this requires yearly development of the high energy beams and the need for high polarization.
  3. The actual running time of the RHIC collider at $\sqrt{s} = 500$ GeV has to be long enough to accumulate the luminosities required before 2013. Years without 500 GeV running will reduce the improvements expected from beam developments and reduce the accumulated luminosity.

  With the projected Luminosity and the FGT upgrade for STAR and the Muon Trigger upgrade for PHENIX it will be possible to meet the milestone.

1.2 Theoretical foundation

The W physics program at RHIC in high-energy polarized proton-proton collisions has been featured in various review articles [1, 2]. Key arguments based on those documents will

be summarized below, before specific aspects of the W kinematics and asymmetries are reviewed, which are essential to motivate the W program both in PHENIX and STAR.

1.2.1 Introduction

Various polarized DIS [3, 4, 5, 6, 7, 8, 9, 10, 11, 12] experiments in combination with constraints given by baryon octet β-decays [13, 14, 15, 16] show that the total quark and anti-quark contribution to the proton spin, summed over all flavors, is surprisingly small.

Inclusive DIS (through γ^* exchange) measurements provide only sensitivity to the combined contributions of quarks and anti-quarks summed over all flavors. However, those measurements cannot provide information on the polarized quark and anti-quark densities separately and in particular the anti-quark polarizations are not determined by inclusive DIS. Direct measurements of individual polarized anti-quark distributions are therefore an important task. It will allow to clarify the overall picture concerning DIS and the β-decays by determining the individual quark and anti-quark contributions by flavor.

Semi-inclusive DIS measurements [17, 18] are one approach to achieving a separation of quark and anti-quark densities. This method combines information from proton and neutron (or deuteron) targets and uses correlations in the fragmentation process between the type of hadron and the flavor of its originating parton, quantified in terms of fragmentation functions. However, the dependence on the details of the fragmentation process limits the accuracy of this method. The experiment E04-113 at Jefferson Laboratory plans to extract quark polarizations, Δu_v, Δd_v and $\Delta\bar{u} - \Delta\bar{d}$, for $x = 0.12 - 0.41$ at $Q^2 = 1.21 - 3.14\,\mathrm{GeV}^2$ based on the measurement of the combined asymmetries $A_{1N}^{\pi^+-\pi^-}$ [19]. Even if the fragmentation functions were perfectly known the low scales of these measurements raise complications about the theoretical uncertainties of the extractions of quark polarizations.

Figure 1 shows the result of a global analysis including both inclusive and semi-inclusive DIS measurements [20]. While the sum of quark and anti-quark distributions, separately shown for u-quarks and d-quarks, is well known, the anti-quark distributions for u-quarks and d-quarks are unconstrained. Results are shown for two different sets of fragmentation functions referred to as KRE [21] and KKP [22]. The result of this global analysis provides yet another argument why further experimental work is needed to improve the accuracy of the knowledge of the $SU(2)$ (u, d) sea.

At RHIC, direct sensitivity to the polarization of $u, \bar{u}, d,$ and $\bar{d}$ quarks in the proton is possible using maximal parity violation for the production of W bosons in $u\bar{d} \to W^+$ and $d\bar{u} \to W^-$ [23, 24, 25, 26, 27, 28, 29, 33].

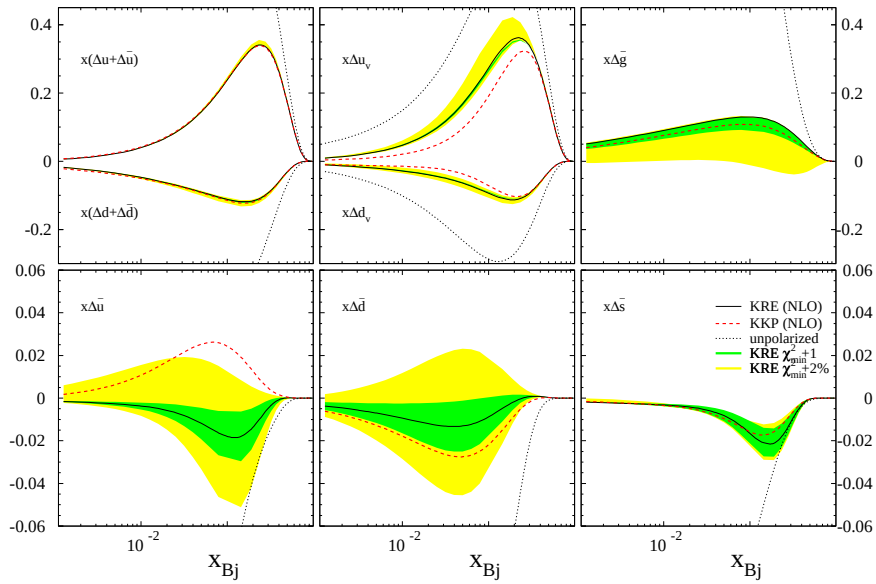

Figure 1: *Parton densitites at $Q^2 = 10\,GeV^2$ along with uncertainty bands corresponding to $\Delta\chi^2 = 1$ and $\Delta\chi^2 = 2\%$ [20].*

In addition to the polarized sector of quark distribution functions, RHIC has the potential to constrain unpolarized quark distribution functions at large Bjorken-x values.

Experiments in recent years have shown [34, 35, 36, 37, 38] a strong breaking of $SU(2)$ symmetry in the anti-quark sea, with the ratio $\bar{d}(x)/\bar{u}(x)$ rising to 1.6 or higher. It is very attractive to learn whether the polarization of $\bar{u}$ and $\bar{d}$ is large and asymmetric as well. Within the chiral quark soliton model based on a $1/N_c$ expansion, it is expected that the polarized flavor asymmetry, $\Delta\bar{u} - \Delta\bar{d}$, is larger than the experimentally established flavor asymmetry in the unpolarized sector [39, 40]. A measurement of the parity-violating asymmetry, A_L, in W production will address the underlying mechanism responsible for the expected polarized flavor asymmetry. RHIC experiments will measure the $\bar{d}/\bar{u}$ unpolarized ratio and the $\bar{u}$ and $\bar{d}$ polarizations separately.

1.2.2 Kinematics and Asymmetries

The following section will review basic aspects of kinematics and asymmetries and follows closely the discussion in [1, 2]. The standard model production of W bosons proceeds through a pure V-A interaction. Thus, the helicity of the incoming quark and anti-quark is fixed. In addition, the W boson couples to a weak charge that correlates directly to flavors. The production of W bosons in proton-proton collisions is dominated by $u, d, \bar{u}$, and $\bar{d}$, with some contamination from $s, c, \bar{s}$, and $\bar{c}$, mostly through quark mixing. Therefore W boson

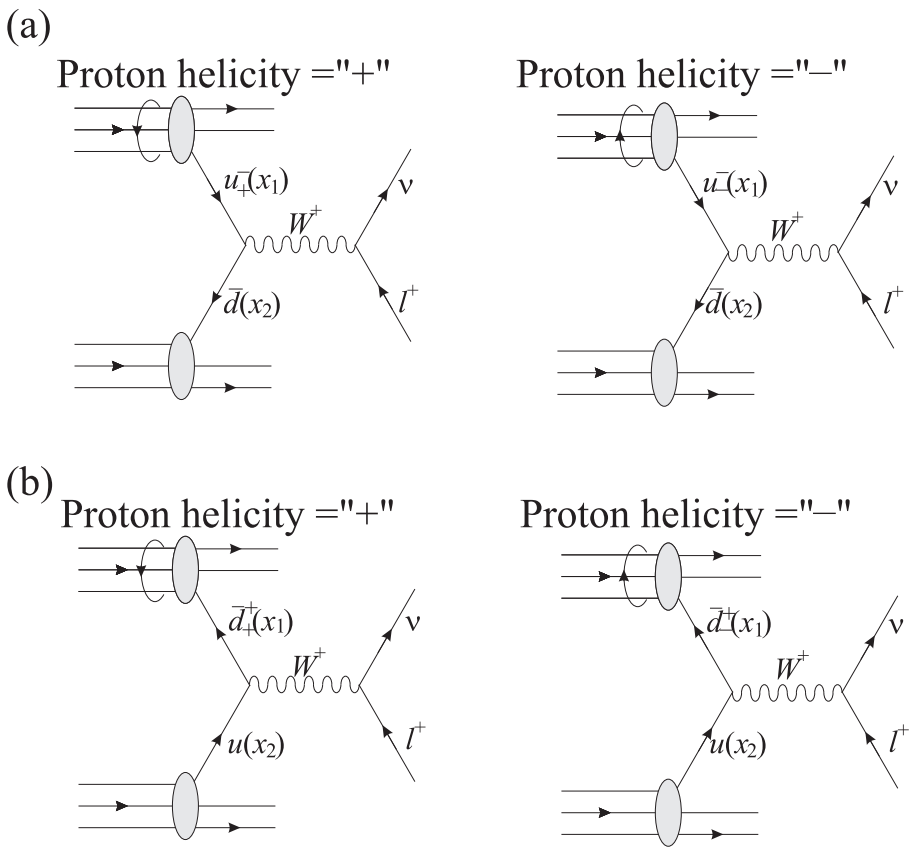

Figure 2: *Production of W^+ bosons in $\vec{p}p$ collisions [1]. (a) Δu is probed. (b) $\Delta\bar{d}$ is probed [1, 2]. The proton on the top in each panel is taken to be the polarized proton, with either positive (left) or negative (right) helicity.*

production is an ideal tool to study the spin-flavor structure of the nucleon. The leading-order production of a W^+ boson, $u\bar{d} \to W^+$, is illustrated in Figure 2.

The cross sections for W^+ and W^- differential in the W boson rapidity y_W and the scattering angle θ^* of the decay lepton in the W center-of-mass system is given as follows:

$$\left(\frac{d^2\sigma}{dy_W d\cos\theta^*}\right)_{W^+} \sim \quad u(x_1)\bar{d}(x_2)(1-\cos\theta^*)^2 + \bar{d}(x_1)u(x_2)(1+\cos\theta^*)^2 \tag{1}$$

and

$$\left(\frac{d^2\sigma}{dy_W d\cos\theta^*}\right)_{W^-} \sim \quad d(x_1)\bar{u}(x_2)(1+\cos\theta^*)^2 + \bar{u}(x_1)d(x_2)(1-\cos\theta^*)^2 \tag{2}$$

Figure 3: *Helicity configuration of W^- (left) and W^+ (right) production showing on top the helicity configuration of the incoming quark and anti-quark. The middle panel shows the direction of the W spin. The lower panel displays the preferred direction of e^-/e^+ quoting the scattering angle θ^* in the W center-of-mass system measured with respect to the positive z axis.*

The characteristic dependence on the θ^* is shown graphically in Figure 3 for the helicity configuration of W^- (left) and W^+ (right) production. This dependence is a direct consequence of the underlying V-A interaction. The top panel shows the helicity configuration of the incoming quark and anti-quark. The middle panel shows the direction of the W spin. The lower panel displays the preferred direction of e^-/e^+ quoting the scattering angle θ^* in the W center-of-mass system measured with respect to the positive z axis.

The momentum fraction carried by the quarks and anti-quarks, x_1 and x_2 (without yet assigning which is which), can be determined from the W boson rapidity y_W as follows:

$$x_1 = \frac{M_W}{\sqrt{s}} e^{y_W}, \quad x_2 = \frac{M_W}{\sqrt{s}} e^{-y_W}. \tag{3}$$

The parity-violating asymmetry is the difference of right-handed ($N^+(W)$) and left-handed ($N^-(W)$) production of W bosons, divided by the sum, normalized by the beam polarization (P):

$$A_L^W = \frac{1}{P} \times \frac{N^+(W) - N^-(W)}{N^+(W) + N^-(W)} \quad . \tag{4}$$

At RHIC, one can determine this asymmetry from either polarized beam, and by summing over the helicity states of the other beam. The production of the left-handed weak bosons violates parity maximally. Therefore, if for example the production of the W^+ proceeded only through the diagram in Figure 2a, the parity-violating asymmetry would directly equal the longitudinal polarization asymmetry of the u quark in the proton:

$$A_L^{W^+} = -\frac{u_-^-(x_1)\bar{d}(x_2) - u_+^-(x_1)\bar{d}(x_2)}{u_-^-(x_1)\bar{d}(x_2) + u_+^-(x_1)\bar{d}(x_2)} = -\frac{\Delta u(x_1)}{u(x_1)}. \tag{5}$$

Similarly, for Figure 2b alone,

$$A_L^{W^+} = -\frac{\bar{d}_-^+(x_1)u(x_2) - \bar{d}_+^+(x_1)u(x_2)}{\bar{d}_-^+(x_1)u(x_2) - \bar{d}_+^+(x_1)u(x_2)} = \frac{\Delta\bar{d}(x_1)}{\bar{d}(x_1)}. \tag{6}$$

In general, the asymmetry is a superposition of the two cases:

$$A_L^{W^+} = -\frac{\Delta u(x_1)\bar{d}(x_2) - \Delta\bar{d}(x_1)u(x_2)}{u(x_1)\bar{d}(x_2) + \bar{d}(x_1)u(x_2)}. \tag{7}$$

To obtain the asymmetry for W^-, one interchanges u and d.

For proton-proton collisions at RHIC with $\sqrt{s} = 500$ GeV, the quark will be predominantly a valence quark. By identifying the rapidity of the W, y_W, relative to the polarized proton, we can obtain direct measures at leading order of the quark and anti-quark polarizations, separated by quark flavor: $A_L^{W^+}$ approaches $-\Delta u/u$ in the limit of $y_W \gg 0$, whereas for $y_W \ll 0$ the asymmetry becomes $\Delta\bar{d}/\bar{d}$.

This picture is valid for the predominant production of W bosons at $p_T \sim 0$. The experimental difficulty is that the W boson is observed through its leptonic decay $W \to l\nu$, and only the charged lepton is observed. The four momenta of the W boson cannot be determined from the momenta of its decay products. Therefore, the rapidity of the W boson cannot be measured directly. It is necessary to relate the lepton kinematics to y_W, so that one can assign the probability that the polarized proton provided the quark or anti-quark. Only then would it be possible to translate the measured parity-violating asymmetry into a determination of the quark or anti-quark polarization at leading order in the proton. As will be shown below, this is only possible in an approximate way provided that the final state lepton is tagged in the forward/backward (Large $|y_l|$) direction.

The rapidity of the W is related to the lepton rapidity in the W rest frame (y_l^*) and in the lab frame ($y_l^{\rm lab}$) by

$$y_l^{lab} = y_l^* + y_W, \quad \text{where} \quad y_l^* = \frac{1}{2}\ln\left[\frac{1+\cos\theta^*}{1-\cos\theta^*}\right]. \tag{8}$$

Here θ^* is the decay angle of the lepton in the W rest frame, and $\cos\theta^*$ can be determined from the transverse momentum (p_T) of the lepton with an irreducible uncertainty of the sign [43], since

$$p_T = p_T^* = \frac{M_W}{2}\sin\theta^*. \tag{9}$$

In this reconstruction, the transverse momentum q_T of the W boson is neglected. In reality, it has a q_T, resulting for example from higher-order contributions such as $gu \to W^+d$ and $u\bar{d} \to W^+g$, or from primordial transverse momentum of initial-state partons. For a given set of y_l and p_T, the above equations imply two solutions y_+ and y_- for y_W. One of them can be correctly chosen if the magnitude of the leptonic rapidity y_l is large.

While it is certainly valuable to determine the asymmetry, $A(y_W)$, in an approximate way in terms of the W boson rapidity in the forward rapidity region of the tagged lepton and relate the so determined asymmetry at leading order to the underlying ratio of polarized and unpolarized distributions functions, the asymmetry, $A(y_W)$, is strongly sensitive to experimental cuts imposed on the observed charged lepton [30]. It has been shown in [30] that the directly measurable asymmetries in terms of the observed charged lepton, $A(y_l)$ and $A(p_T)$, are a viable alternative to the asymmetry $A(y_W)$. The theoretical framework on the measurement of the longitudinal single-spin asymmetry as a function of the leptonic rapidity is well developed and has been presented in [30]. Reliable predictions are provided based on resummation calculations. These calculations have been incorporated in a Monte-Carlo program called RHICBOS. This framework will be the basis for a full global analysis to extract polarized quark and anti-quark distribution functions with charged lepton asymmetries, $A(y_l)$ and $A(p_T)$, as input [44].

Usually W production is identified by requiring charged leptons with large p_T and large missing transverse energy, due to the undetected neutrino. Since none of the detectors at RHIC are hermetic, measurement of missing p_T is not available, which leads to some background. Possible sources of leptons with high p_T include charm, bottom, and vector boson production. Above $p_T \geq 20$ GeV/c, leptons from W decay dominate, with a small contribution from Z^0 production. The additional background from misidentified hadrons is expected to be small at high p_T. This will be discussed in further detail later.

The sensitivity has been estimated using the RHICBOS MC program [30] based on a calculation for Q_T resummation of large logarithmic contributions originating from multiple soft gluon contribution. This framework allows the prediction of the leptonic longitudinal single-spin asymmetry for various distribution functions taking into account the impact of leptonic cuts such as p_T. The sensitivity to different distribution functions of the underlying quark and anti-quark distributions based on GRSV-STD, GRSV-VAL [31] and GS-A [41] and others are shown in Fig. 4. GRSV-VAL considers a flavor asymmetric scenario of Δu and Δd whereas GRSV-STD is based on a flavor symmetry description. Clear discrimination power to the choice of the underlying distribution function is seen in the forward direction in case of W^- production. For W^+ production, the sensitivity is similar in the forward and central region.

Despite the fact that the forward direction comprises a small fraction of the W production cross section, it is an essential part of the measurement. As described above, models show significant discriminating power in the forward direction, especially for W^- production. Moreover this kinematic region allows to connect the detected lepton back to the W production kinematics, and the sea quark polarization.

The asymmetries to be expected in the corresponding detector parts of PHENIX and STAR are shown in Fig. 5 as a function of the lepton rapidity and in 6 as a function of the lepton transverse momentum p_T. The large differences seen in Fig. 4 are still present and are even more pronounced at large transverse momenta.

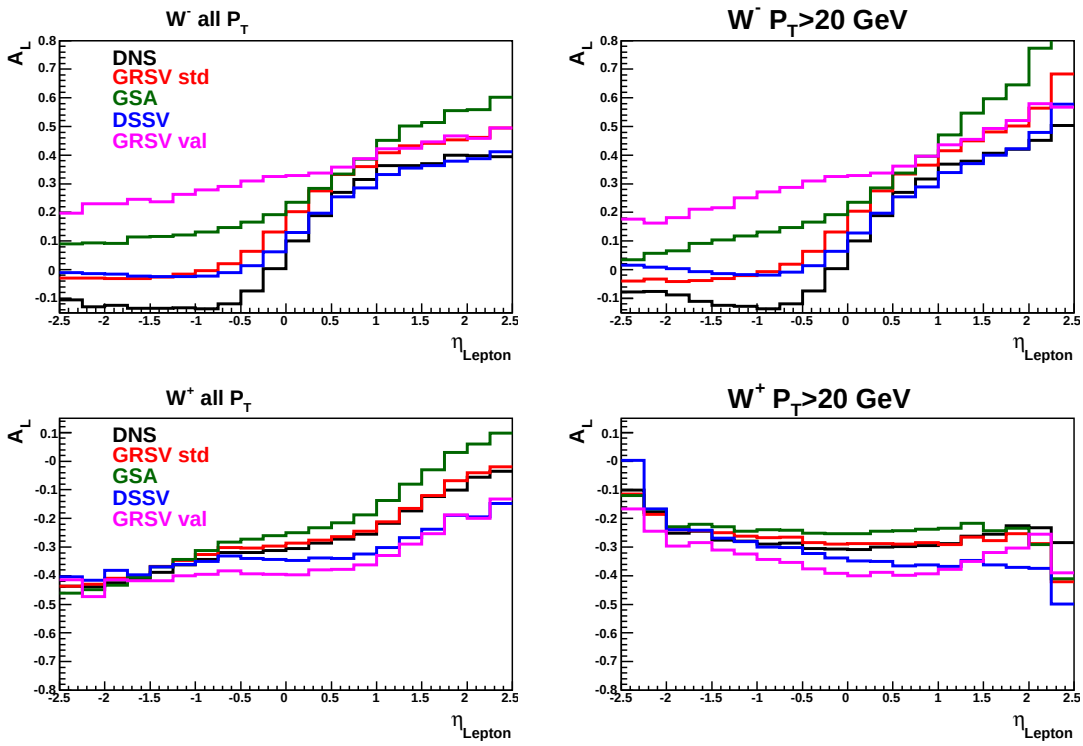

Figure 4: *Inclusive asymmetries A_L obtained by RHICBOS [30] for the polarized parton distribution functions GRSV standard, GRSV valence [31], DSSV [32], Gehrmann-Sterling A [41], DNS [20] and AAC03 [42]. Left figure: $A_L^{l^-}$ (top plot) and $A_L^{l^+}$ (bottom plot) as a function of the lepton rapidity y without a cut on the lepton's transverse momentum. Right figure: $A_L^{l^-}$ (top plot) and $A_L^{l^+}$ (bottom plot) as a function of the lepton rapidity y with $p_T > 20$ GeV.*

Figures 7 and 8 show the approximate x_1, x_2 dependences in the different acceptance regions based on the rapidity of the W displayed as function of either the lepton rapidity or its transverse momentum p_T. A clear correlation of the sensitivities can still be seen at the different lepton transverse momenta and rapidities and it will be possible to probe quark polarizations at relatively high x and antiquark polarizations at smaller x at a high scale.

The acceptance in x_1 for the valence d-quark reaches more than 0.65 so that one obtains sensitivity to the high-x behavior of the d polarization. Power-counting rules [45] suggest that $\Delta d(x)$ has to change its sign from negative values to approach 1 at x going to 1. It is not completely clear at what x the sign of $\Delta d(x)$ has to change and if it really changes. However, such a turnaround would be visible at the highest lepton rapidities at RHIC. As can be seen in Fig. 9 the rising trend of the asymmetry with increasing rapidity would be dampened or even start decreasing again.

As the scale of the quark and antiquark polarization measurements is basically the

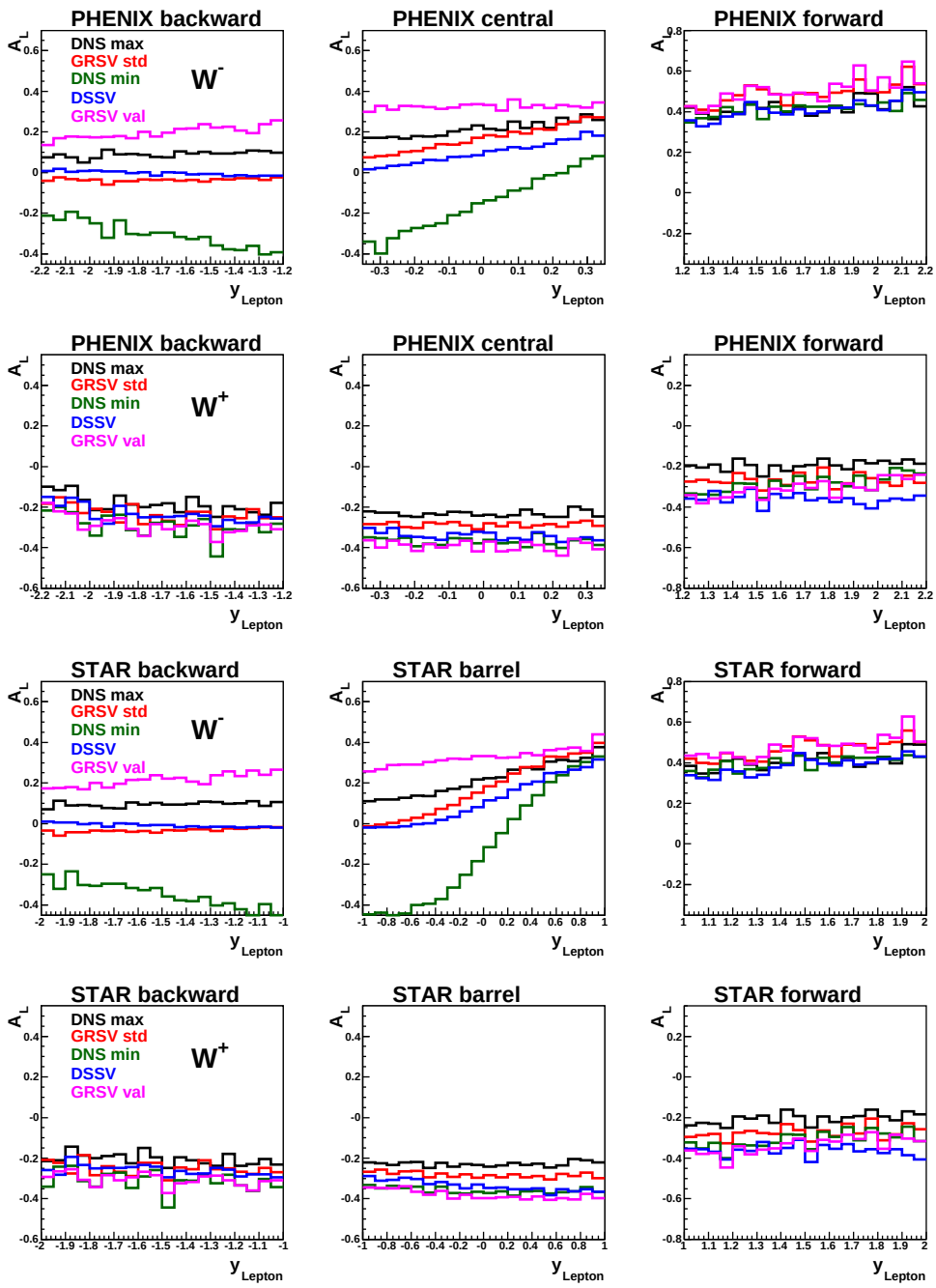

Figure 5: *Inclusive asymmetries A_L obtained by RHICBOS [30] for the polarized parton distribution functions GRSV standard, GRSV valence [31], DSSV [32], and DNS [20] using a maximal and minimal sea polarization scenario. The asymmetries $A_L^{l^-}$ and $A_L^{l^+}$ as a function of the lepton rapidity η_{Lepton} with $p_T > 20$ GeV are shown in the different detector regions.*

mass of the produced W ($Q^2 \sim 6400$ GeV^2) one also obtains a large lever arm for the QCD evolution. All exsiting measurements were made at significantly lower scales. This will

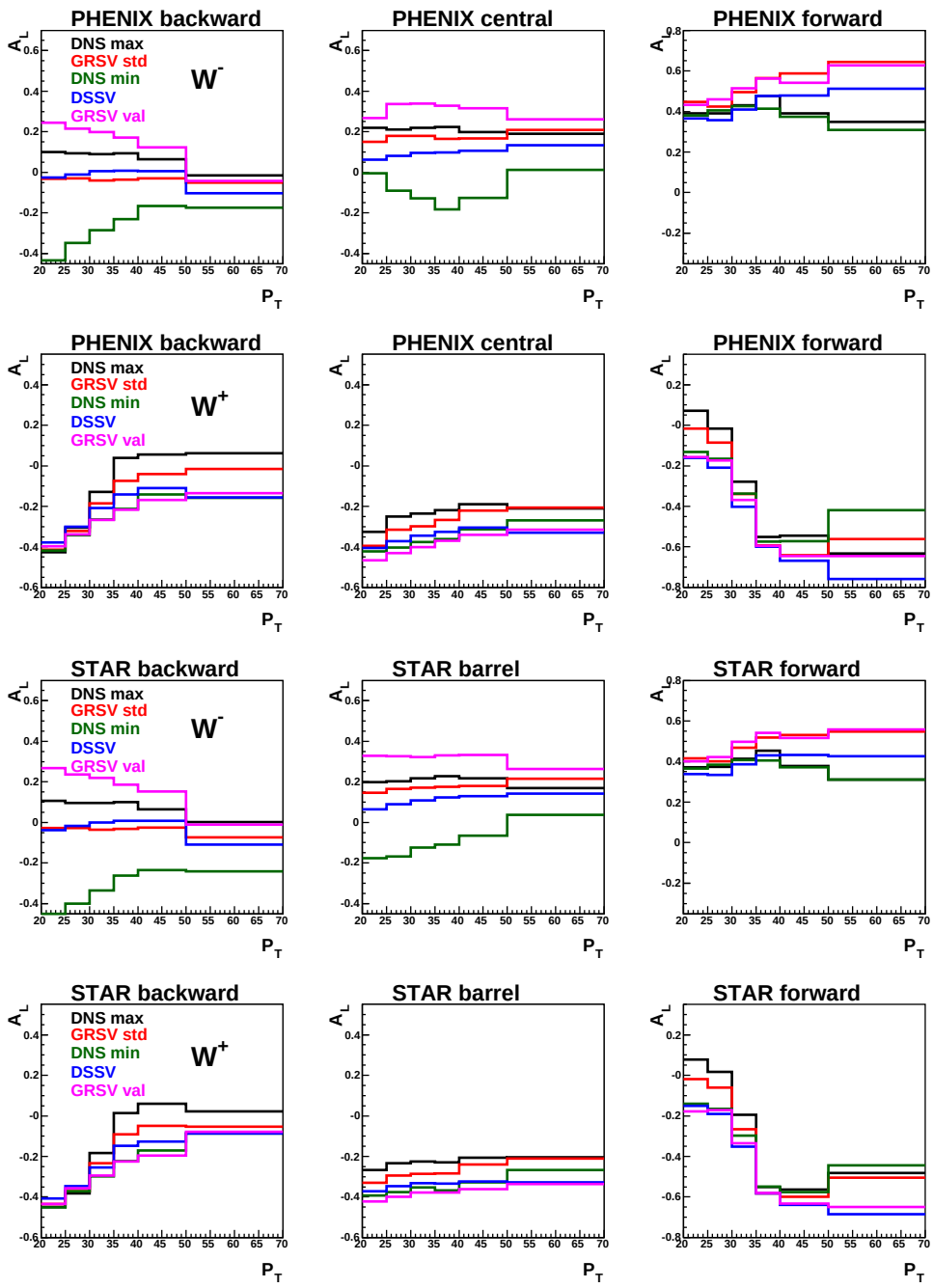

Figure 6: *Inclusive asymmetries A_L obtained by RHICBOS [30] for the polarized parton distribution functions GRSV standard, GRSV valence [31], DSSV [32], and DNS [20] using a maximal and minimal sea polarization scenario. The asymmetries $A_L^{l^-}$ and $A_L^{l^+}$ as a function of the lepton transverse momentum p_T with $p_T > 20$ GeV are shown in the different detector regions.*

provide an additional constraint on the gluon polarization, which can be extracted from

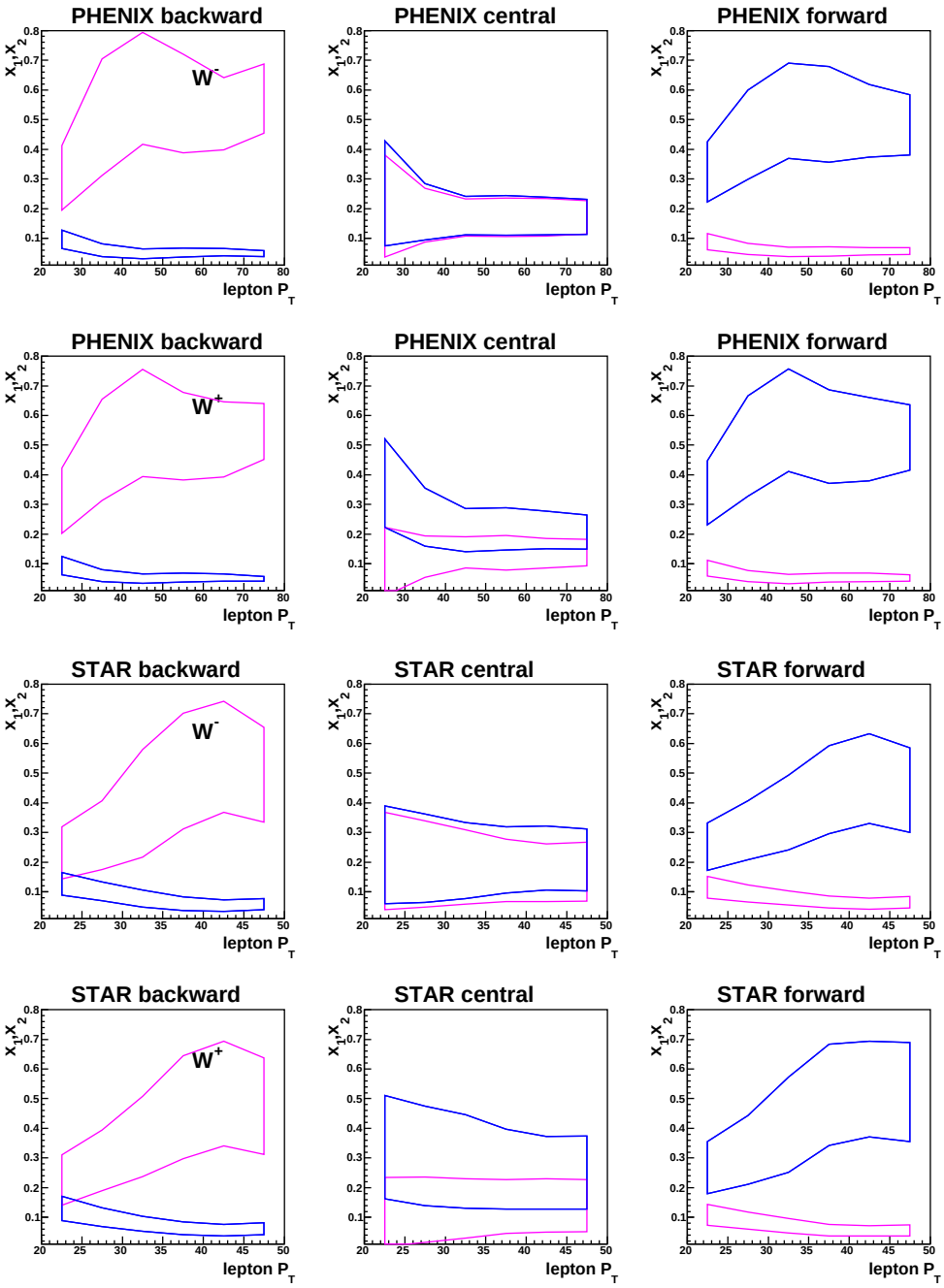

Figure 7: *Average regions of x_1 (blue lines) and x_2(purple lines) in the different detector ranges using RHICBOS [30] as a function of the lepton transverse momentum p_T. The range was calculated by the average value and taking the RMS on the corresponding x distributions.*

the evolution. Figure 10 shows the impact of different gluon polarization scenarios on the expected asymmetries as evolved to the W scale.

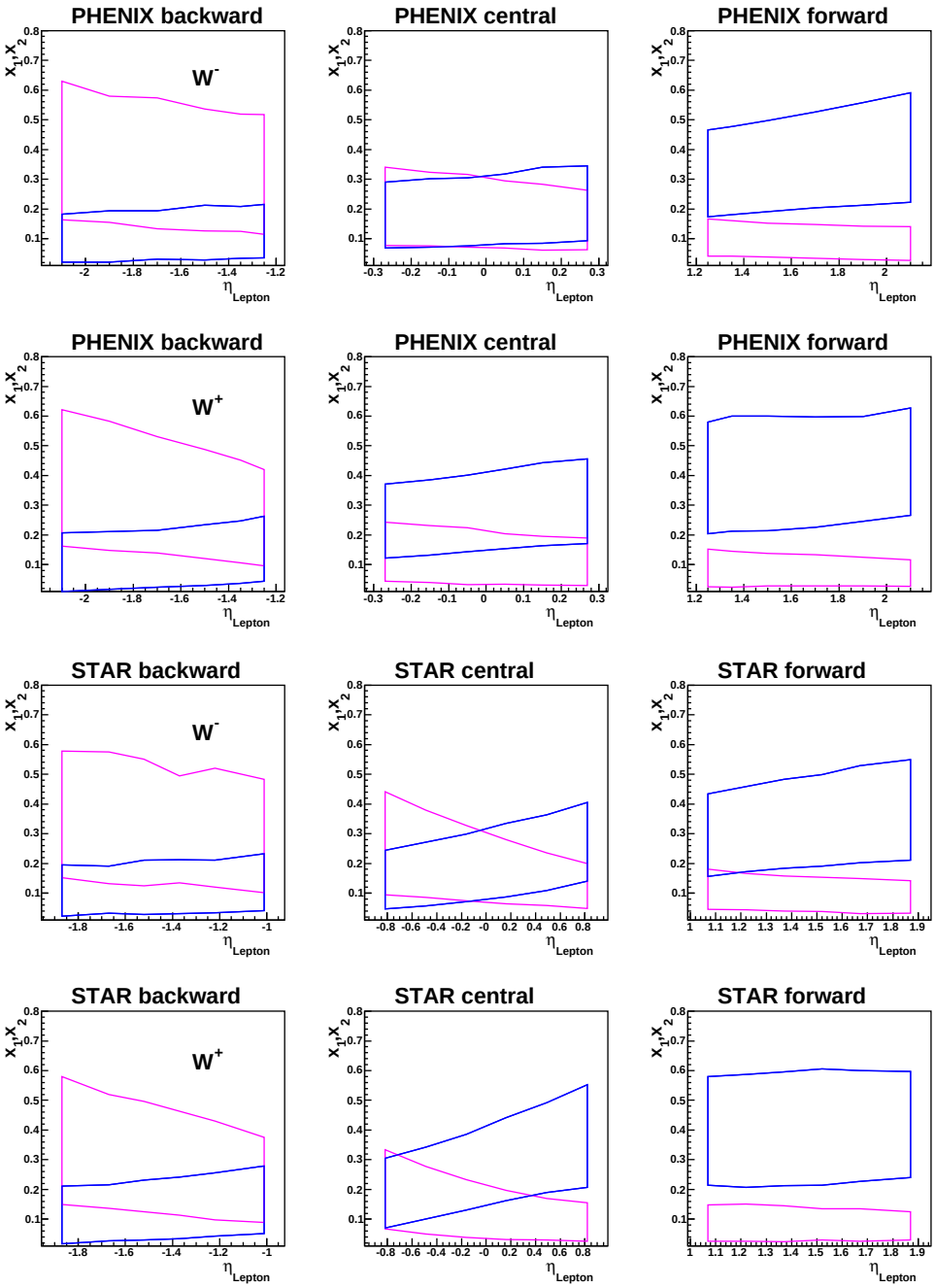

Figure 8: *Average regions of x_1 (blue lines) and x_2(purple lines) in the different detector ranges using RHICBOS [30] as a function of the lepton rapidity η_{Lepton}. The range was calculated by the average value and taking the RMS on the corresponding x distributions.*

1.3 Measurement of flavor asymmetry of light sea quarks in nucleon

Sea quark distributions are difficult to calculate from first principles. Therefore, various models have been proposed to describe sea quarks in the nucleon. The earliest models

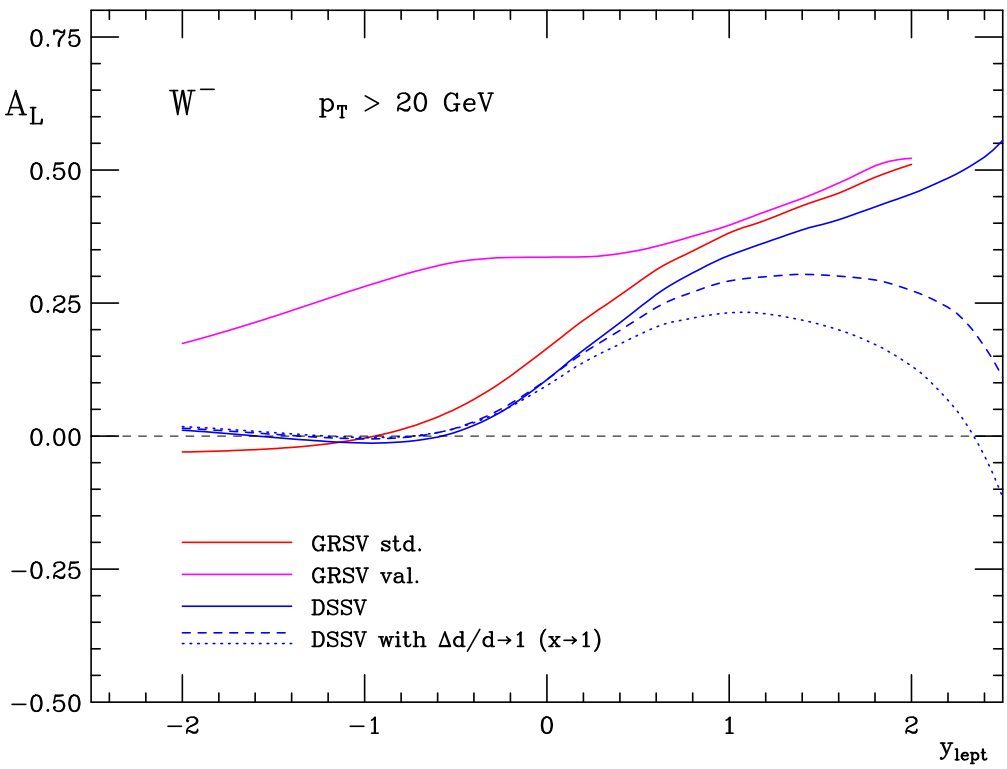

Figure 9: *Inclusive single spin asymmetries A_L for negative leptons as a function of the lepton rapidity η_{Lepton} in LO approximation. The Asymmetries shown are for DSSV (blue line), DSSV but requiring a zero crossing toward 1 at $x = 0.67$(dashed line) and at $x = 0.55$ (dotted line), GRSV standard (red line) and valence (purple line).*

have assumed flavor symmetry of sea quarks in the nucleon. Since this assumption was not based on any known symmetries, it remained to be tested by experiments.

It has already been shown by neutrino-induced charm production experiments [56] [57] that the strange quark content in the nucleon is not as large as up and down sea quarks. This asymmetry can be attributed to the large mass difference between strange quark and up and down quarks. For the light up and down quarks, it was still possible that their distributions in the nucleon sea are symmetric. To test the flavor symmetry of the up and down quarks in the nucleon sea, one can measure the Gottfried sum [58]:

$$S_G = \int_0^1 [F_2^{\mu p}(x) - F_2^{\mu n}(x)]dx = \frac{1}{3} + \frac{2}{3}\int_0^1 [\bar{u}(x) - \bar{d}(x)]dx. \tag{10}$$

In Eq. 10, S_G equals $1/3$ if $\bar{u}(x)$ and $\bar{d}(x)$ are identical. Early experiments [59, 60, 61] suffered from large systematic errors and could not reach a definite conclusion, although they consistently showed a value below $1/3$.

More recently, the NMC collaboration reported a measurement on the Gottfried sum with muon DIS data in the 1990s. Their measurement covered the smaller x region (down

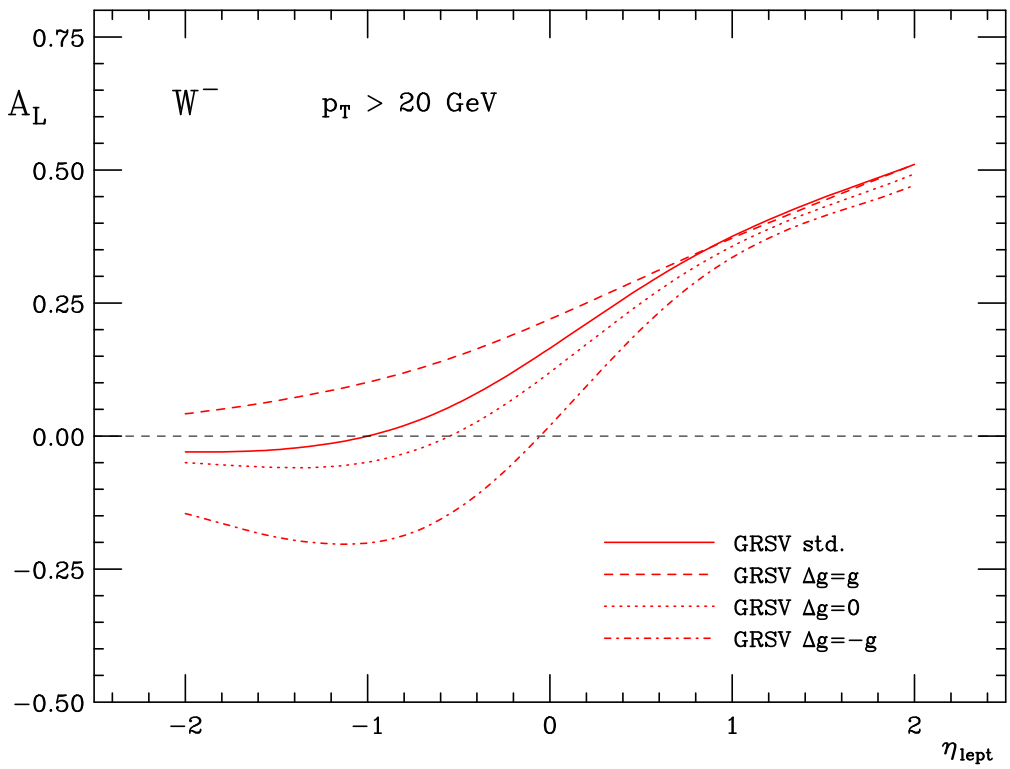

Figure 10: *Inclusive single spin asymmetries A_L for negative leptons as a function of the lepton rapidity η_{Lepton} in LO approximation. The Asymmetries shown are for GRSV including a maximal gluon polarization (dashed line),a minimal gluon polarization (dash-dotted line), zero gluon polarization (dotted line) and the best fit (std,continous line) evolved to $Q^2 = 6400$ GeV^2.*

to 0.004), allowing an accurate determination of $S_G = 0.235 \pm 0.026$ [62]. This result provided the first strong evidence that $\bar{u}(x) \neq \bar{d}(x)$.

Following the NMC measurement, the $\bar{d}/\bar{u}$ ratios as a function of x were measured using other experimental techniques. These new measurements include the NA51 [63] and E866 [64] experiments with the Drell-Yan process and the HERMES experiment [65] with semi-inclusive deep inelastic scattering. The $\bar{d}/\bar{u}$ asymmetry is clearly established from these experiments.

Various theoretical models have been proposed to explain the $\bar{d}/\bar{u}$ asymmetry. Review articles [66, 67, 68] have detailed descriptions on these models. Many models, e.g. meson-cloud model, chiral quark model, and soliton model, attribute the flavor asymmetry to the presence of isovector mesons (especially the pions). Other models such as instanton models, lattice gauge approach and Pauli-blocking model, consider the effects of the valence quarks on the quark-antiquark sea. While these models are capable of describing the $\bar{d} - \bar{u}$ data, significant difficulties are encountered to reproduce the $\bar{d}/\bar{u}$ data at $x > 0.2$, where

the E866 data suggest a rapid fall-off of this ratio.

To better determine mechanisms which generate the flavor asymmetric nucleon sea, it is necessary to extend the x range of existing $\bar{d}/\bar{u}$ ratio measurements. At the high x region, Drell-Yan experiments at the new 120 GeV Fermilab Main Injector (E906) and at the 50 GeV J-PARC have been proposed. At the other end of x range, Drell-Yan measurement at RHIC could extend the present knowledge on the $\bar{d}/\bar{u}$ ratio down to around $x = 10^{-3}$, which is an order of magnitude lower than the E866 experiment.

At RHIC, W production in pp collisions could provide an independent measurement of the $\bar{d}/\bar{u}$ ratio. The differential cross section for W^+ production in pp collision is proportional to [69]

$$\cos^2\theta_c[u(x_1)\bar{d}(x_2) + \bar{d}(x_1)u(x_2)] + \sin^2\theta_c[u(x_1)\bar{s}(x_2) + \bar{s}(x_1)u(x_2)]. \tag{11}$$

where $u(x)$, $d(x)$, $s(x)$ are the distribution functions for up, down and strange quarks in the proton. By interchanging u with $\bar{u}$, d with $\bar{d}$, one obtains the expression for W^- production.

An observable directly related to the $\bar{d}/\bar{u}$ ratio is the ratio of the differential cross sections for W^+ and W^- production. Given the fact that the contribution from strange quarks is small, this ratio can be derived from Eq. (11)(and charge conjugated):

$$R(x_F) \equiv \frac{\frac{d\sigma}{dx_F}(pp \to W^+ + X)}{\frac{d\sigma}{dx_F}(pp \to W^- + X)} \approx \frac{u(x_1)\bar{d}(x_2) + \bar{d}(x_1)u(x_2)}{\bar{u}(x_1)d(x_2) + d(x_1)\bar{u}(x_2)}. \tag{12}$$

$R(x_F)$ is clearly symmetric with respect to $x_F = 0$, where $x_F = x1 - x2$. At the kinematic region $x_F \gg 0$, where $x_1 \gg x_2$, the ratio can be approximated as

$$R(x_F \gg 0) \approx \frac{u(x_1)}{d(x_1)}\frac{\bar{d}(x_2)}{\bar{u}(x_2)}. \tag{13}$$

while at $x_F = 0$, the ratio is

$$R(x_F = 0) \approx \frac{u(x)}{d(x)}\frac{\bar{d}(x)}{\bar{u}(x)}. \tag{14}$$

Eqs. (13) and (14) show that a measurement of W^+ relative to W^- production in pp collision allows a direct determination of $\bar{d}/\bar{u}$, provided that the value of u/d is known. One advantage is that one obtains this ratio directly without the need of nuclear targets. In PHENIX and STAR the x_F coverage for W production is very broad. To illustrate the sensitivity of $R(x_F)$ to the $\bar{d}/\bar{u}$ ratio, Fig. 11 shows the calculations for pp collisions at $\sqrt{s} = 500$ GeV using the MRS S0', MRST, CTEQ5, and GRV98 PDFs.

At $x_F = 0$, which corresponds to $x_1 = x_2 = 0.16$, the $\bar{d}/\bar{u}$ ratio is well determined to be $\simeq 2.0$. Eq. 14 shows that $R(x_F = 0) \simeq 2\bar{d}/\bar{u}(x = 0.16)$. Fig. 11 shows that, $R(x_F = 0)$ for the $\bar{d}/\bar{u}$ asymmetry MRST, CTEQ5, and GRV98, all have very similar predictions. In

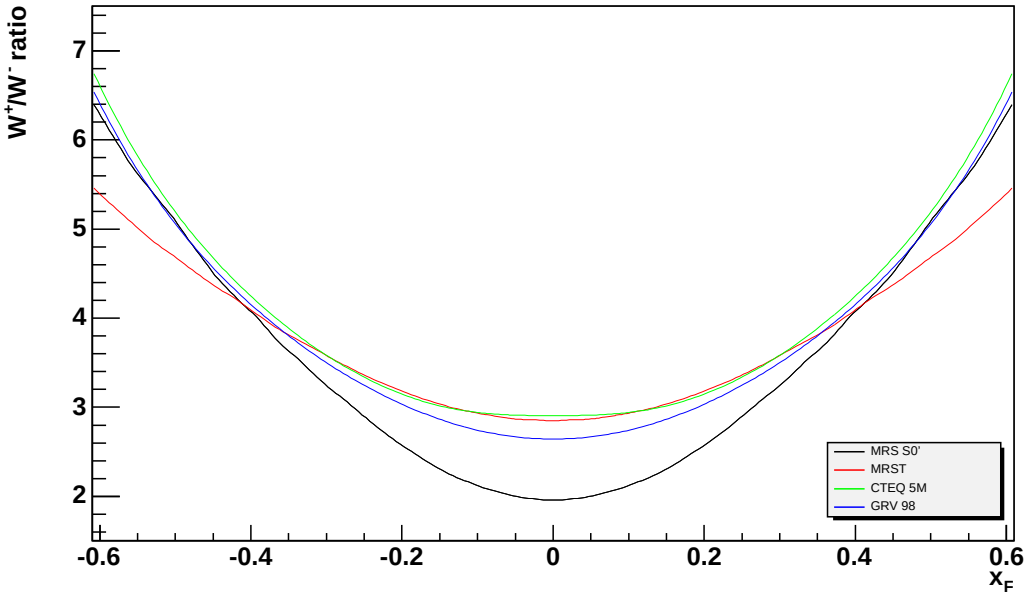

Figure 11: *Prediction of the ratio $R(x_F)$ of W production in pp collisions at RHIC ($\sqrt{s} = 500$ GeV) using the MRS S0', MRST, CTEQ5, and GRV98 PDFs.*

contrast, the calculation using MRS S0', which has symmetric $\bar{d}$, $\bar{u}$ distributions, gives a significantly lower value for $R(x_F = 0)$: $R(x_F = 0) \simeq 2$.

A distinct advantage of extracting the $\bar{d}/\bar{u}$ ratio from W boson production in pp collision is that no correction for the nuclear effect in the deuteron and no assumption on the validity of charge symmetry (i.e. $u_p = d_n$, $u_n = d_p$, $\bar{u}_p = \bar{d}_n$, etc) is required. This is in contrast to the Drell-Yan experiments and the Gottfried-sum measurement, which require nuclear binding corrections on the effect in the deuteron and the assumption of charge symmetry to relate the neutron with the proton parton distributions. It is also worth noting that the $\bar{d}/\bar{u}$ ratio extracted from W boson production explores the symmetry of nucleon sea at a very large value of Q^2 ($Q^2 = m_W^2 \simeq 6400$ GeV^2). A comparison with $\bar{d}/\bar{u}$ obtained from E866 Drell-Yan would reveal how the sea quark asymmetry evolves with the Q^2 scale.

At large x_F, x_2 becomes small, and $x_F \simeq x_1$. Therefore, $R(x_F \gg 0)$ probes u/d at large x as well as $\bar{d}/\bar{u}$ at small x (see Eq. 13). The value of $\bar{d}/\bar{u}$ at small x are quite well determined from the E866 Drell-Yan measurement. In fact, one expects $\bar{d}/\bar{u} \to 1$ as $x \to 0$ from perturbative QCD. Therefore, the main interest for measuring W^+/W^- ratio at large x_F in PHENIX is to determine the u/d ratios at large x. As discussed in a later section, the u/d ratio at large x is still poorly determined experimentally and remains a very interesting topic to study at RHIC.

A detailed simulation code has been written to calculate the W production cross sections and the expected statistical accuracy for measuring the W^+/W^- ratio in PHENIX. This code can reproduce the W and Z boson production cross sections measured at UA2 and CDF. The differential cross section for W production at RHIC energy is shown in Fig. 12. This code also takes into account the $W^\pm \to l^\pm \mu$ decay. The experimental observable in PHENIX is the l^+/l^- ratio as a function of the rapidity y of the charged leptons. The expected l^+/l^- and the statistical uncertainties for an integrated pp luminosity of 950 pb^{-1} are also shown for several different PDFs. The acceptance of the muon arms has been included in the calculation. Fig. 13 clearly demonstrates that the W production data anticipated at PHENIX has a sufficient accuracy to test the $\bar{d}/\bar{u}$ asymmetry in the nucleon sea.

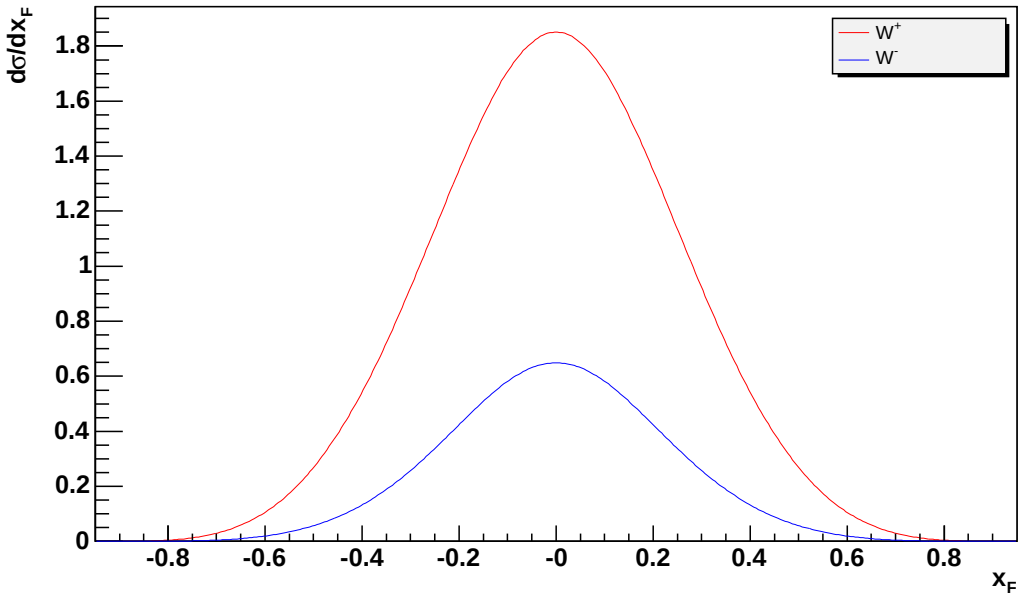

Figure 12: *Differential cross section for W production at RHIC ($\sqrt{s} = 500$ GeV) as a function of x_F calculated using MRST.*

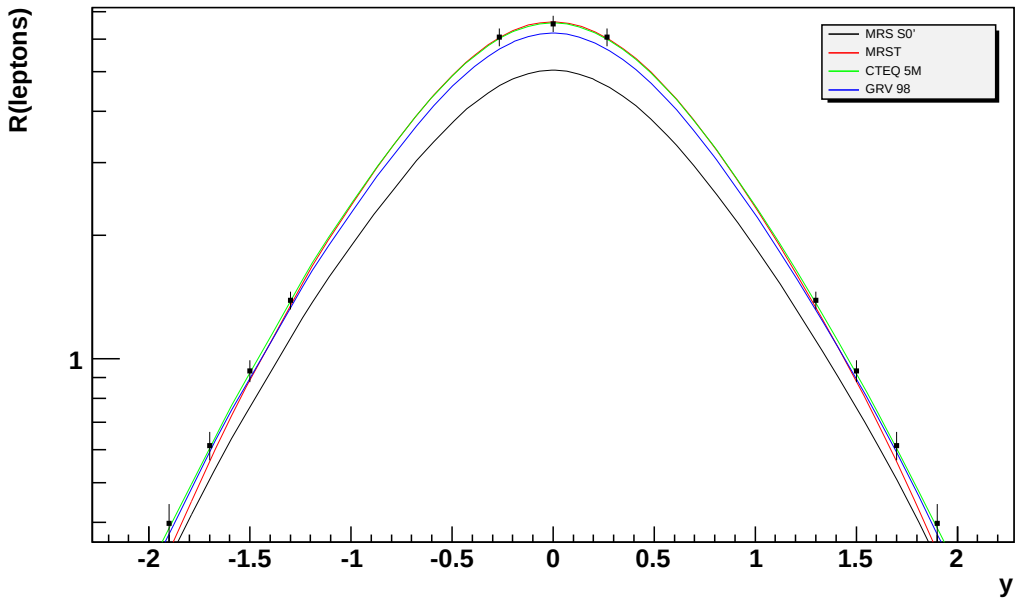

Figure 13: *The data points correspond to the expected l^+/l^- ratio and its statistical uncertainty in the PHENIX detector for 950 pb^{-1} as a function of charged lepton rapidity y. The four curves correspond to the l^+/l^- ratio predicted by MRS S0', MRST, CTEQ5, and GRV98 PDFs.*

2 W physics program at STAR

2.1 Forward region

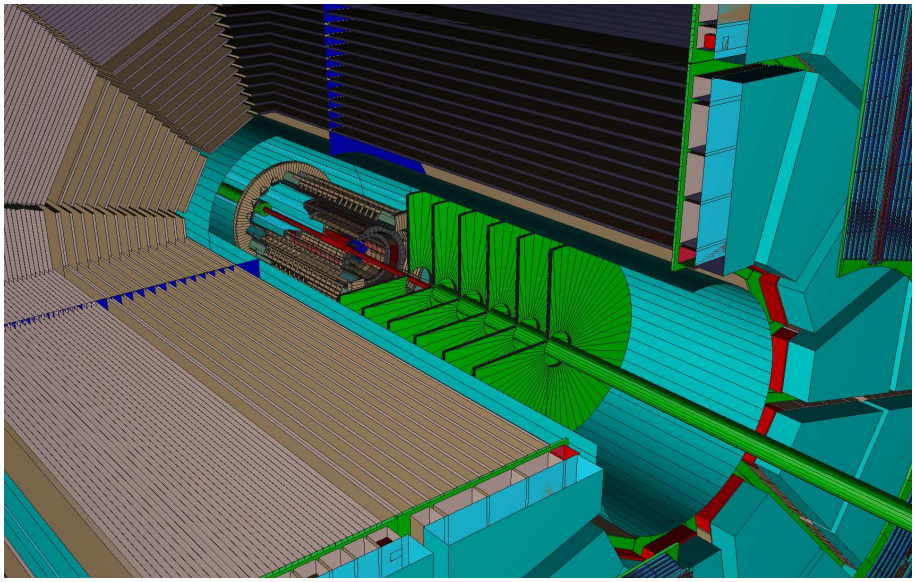

Figure 14: *3D-view of the STAR inner and forward tracking region as implemented in the GEANT model of the STAR detector (STARSIM).*

The STAR collaboration is preparing a tracking detector upgrade to further investigate fundamental properties of the new state of strongly interacting matter produced in relativistic-heavy ion collisions at RHIC and to provide fundamental studies of the proton spin structure and dynamics in high-energy polarized proton-proton collisions at RHIC. The STAR forward tracking upgrade, specifically the Forward GEM Tracker (FGT), will focus on novel spin physics measurements in W production in high-energy polarized proton-proton collisions. The FGT project has been reviewed by the BNL Detector Advisory Board in January 2007 and was recommended to be pursued on an aggressive schedule. The total project cost is estimated to be below $2 million, which will allow for an accelerated construction and installation. The actual review of the FGT project organized by BNL and STAR occurred in January 2008 and resulted in the recommendation to fund the FGT effort through capital equipment funds.

Measurements aimed at determining the flavor dependence ($\Delta\bar{u}$ versus $\Delta\bar{d}$) of the polarized sea are a primary future goal of the STAR spin program. The production of $W^{-(+)}$ bosons provides an ideal tool to study the spin-flavor structure of the proton. $W^{-(+)}$ bosons can be detected through their leptonic decays, $e^- + \bar{\nu}_e\,(e^+ + \nu_e)$, where only the respective charged lepton is measured. Forward scattered $e^{-(+)}$ tagged in the STAR Endcap ElectroMagnetic Calorimeter (EEMC) ($1 < \eta < 2$) with the incoming polarized proton beam moving toward (away) from the STAR EEMC, yield a purity for $W^{-(+)}$ coming from

$\bar{u}+d$ $(\bar{d}+u)$ quarks of about 98% (75%) [46]. The STAR EEMC region provides additional way to constrain to constrain polarized quark distribution functions in W production. The charge sign discrimination probability is clearly adequate at mid-rapidity as well as the STAR BEMC to provide e/h separation by at least two order of magnitude. However, the focus of the following discussion is based on the STAR EEMC acceptance region.

The discrimination of $\bar{u}+d(\bar{d}+u)$ quark combinations requires distinguishing between high p_T $e^{-(+)}$ through their opposite charge sign, which in turn requires precise tracking information. An upgrade of the STAR forward tracking system is needed to provide the required tracking precision for charge sign discrimination. This upgrade will consist of six triple-GEM detectors with two dimensional readout arranged in disks along the beam axis (Z), referred to as the Forward GEM Tracker (FGT).

Figure 14 shows a 3D-view of the STAR inner and forward tracking region as implemented in the GEANT model of the STAR detector (STARSIM). The set of six triple-GEM disks can be clearly seen. Figure 15 shows a 3D-view of the FGT as modeled by the mechanical engineering design tool SolidWorks. The GEM disks will sit inside the inner field cage of the STAR Time Projection Chamber (TPC), and have an outer radius of 38.6 cm and an inner radius of 10.5 cm. Each triple-GEM disk is subdivided into quarter sections whose boundaries are aligned with respect to the TPC sector and EEMC boundaries. All mechanical details and gas piping have been implemented along with the design of a new west support structure.

The charge-sign discrimination of high-p_T $e^{-(+)}$ to distinguish $W^{-(+)}$ bosons in the range $1 < \eta < 2$ will be based on using a beam line constraint, precise hit information from six triple-GEM disks, hits from the TPC, and the electromagnetic cluster data from the shower-maximum detector of the STAR EEMC. Information from the existing detectors (without the FGT) is insufficient. Furthermore, the separation of $e^{-(+)}$ from hadronic background will be important and therefore the full exploitation of the STAR EEMC with its intrinsic means for e/h separation (pre-shower and post-shower readout system) will be crucial. The charge sign determination of forward scattered $e^{-(+)}$, tagged in the STAR EEMC in polarized proton-proton collisions is the main motivation for the STAR forward tracking upgrade.

Several options have been studied based on disk and barrel arrangements. The proposed configuration based on six triple-GEM disk detectors addresses several issues such as optimized acceptance taking into account the position of the collision vertex along the beam axis (Z) with a Gaussian sigma of about 30 cm. It has been shown that a disk configuration is preferred in terms of acceptance and resolution in comparison to a barrel configuration, in particular at large η. The proposed configuration provides a rather cost effective solution based only on triple-GEM technology. The usage of additional silicon disks at smaller radii does not yield an improvement in performance. Precise hit information from the fast inner tracking system (Silicon Strip Detector or SSD and the proposed Intermediate Silicon Tracker or IST) is useful to enhance the acceptance away from the

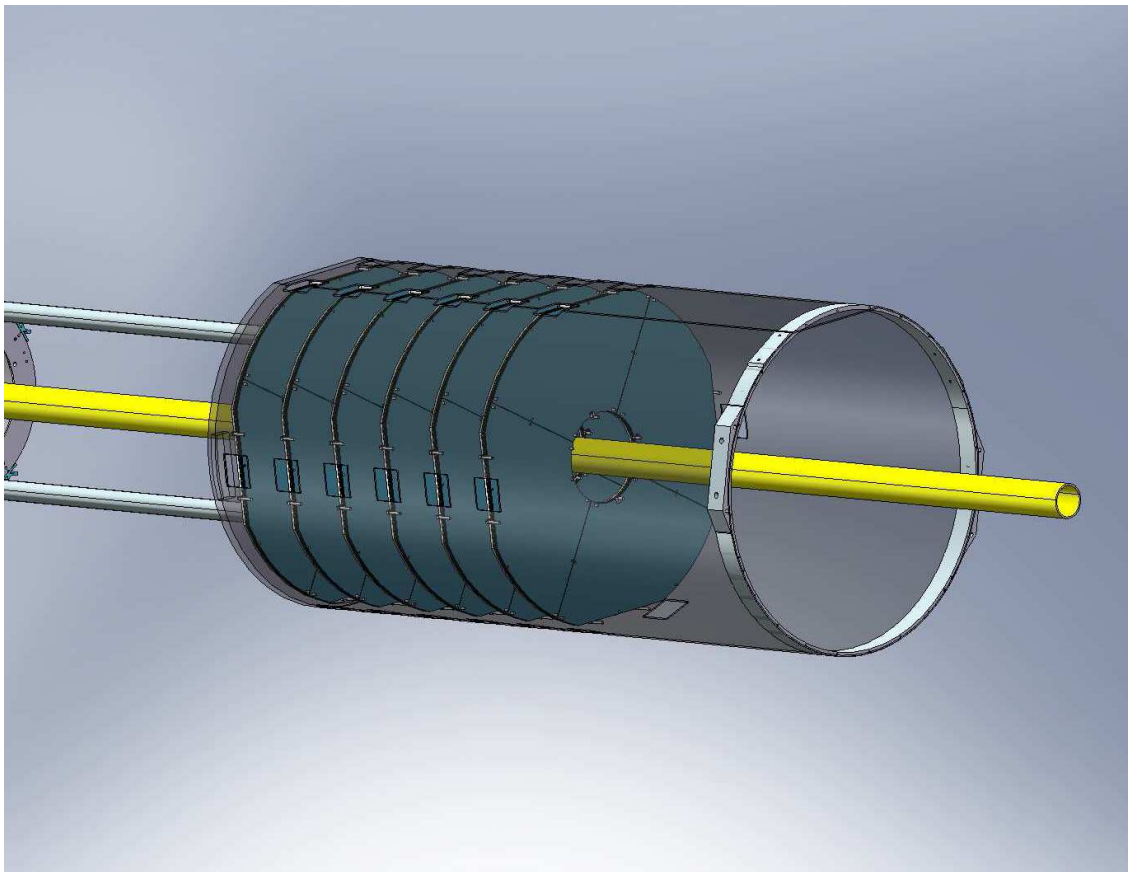

Figure 15: *3D-view of the FGT as modeled by the mechanical engineering design tool called SolidWorks.*

FGT and the center of STAR ($Z < 0$).

A number of simulations have been performed in developing the FGT layout to optimize the overall FGT geometry, the number and location of planes, to assure high charge sign discrimination efficiency. In additions, several studies have been performed to optimize the readout strip geometry along with studies concerning the charge collection in the GEM chambers which will eventually be used for developing tracking and vertex finding algorithms in the full multi-particle pileup environment expected in real events. Initial studies of e/h discrimination have been performed based on full W and QCD background MC samples.

Figure 16 shows the charge discrimination probability (ratio of the number of reconstructed tracks with the correctly reconstructed charge sign divided by the number of generated tracks) for the case of: a) only the TPC and vertex constraint, b) as in a) but adding the EEMC SMD and c) as in b) and including the FGT, SSD and IST. The TPC only case shows a clear drop in the charge discrimination probability for $\eta > 1.3$. The impact of the EEMC SMD can be seen by comparing Figure 16 a) and Figure 16 b). The need for

additional precise hits from the FGT is clearly apparent from a comparison of Figure 16 b) and Figure 16 c). A number of variations about our optimum design and anticipated performance have been considered to test the robustness of the resulting charge sign discrimination of high-p_T tracks in the STAR EEMC acceptance region. It has been shown that this task can be accomplished using a beam line constraint, precise hit information from six triple-GEM disks, hits at forward η from the TPC and the electromagnetic-cluster hit information from the shower-maximum detector of the STAR EEMC. The proposed configuration provides optimized acceptance for a Z vertex distribution width of about 30 cm. Precise hit information from the fast inner tracking system (IST and SSD) is useful to enhance the acceptance for $Z < 0$. However, those hits are not mandatory for the physics program as presented in this proposal. The proposed configuration provides a cost effective solution based on GEM technology only.

GEM technology is widely employed by current and future experiments in nuclear and particle physics. A SBIR[1] proposal [47] (Phase 1 and Phase 2) has been approved and is the basis for the development of the industrial production of GEM foils to be used for the forward GEM tracking system [48]. The proposed configuration is based on light-weight materials to limit the amount of dead material in the forward direction.

The challenge of e/h discrimination is illustrated in Figure 17. The p_T distributions for charged hadrons from a PYTHIA MC sample are shown in comparison to a PYTHIA MC sample of electrons from W events. Even at the peak of the W^- decay distribution near p_T = 40 GeV there are $\approx$300 times more hadrons than electrons. The situation clearly gets worse with lower p_T. Figure 17 also demonstrates that a drastic reduction in background can be achieved while retaining most of the W signal events by requiring isolation cuts and a 'missing p_T' cut (actually a veto on energy opposite the electron candidate in ϕ), and at 40 GeV these appear nearly sufficient. A reduction of hadronic background by at least two orders of magnitude is expected.

The STAR EEMC provides a powerful set of individual calorimeter elements for efficient e/h discrimination through transverse and longitudinal shower shape discrimination. Figure 18 shows a typical shower for a 30 GeV electron. Electrons form a shower contained in approximately one Moliere radius beginning at the first layers of the calorimeter building to a large number of particles at the shower maximum detector and decreasing toward the back of the calorimeter. The calorimeter is only one hadron interaction length deep and hadrons can pass through the EEMC with a MIP response only. In case a hadronic shower does develop, a large diffuse shower is produced and significant energy leaves the rear of the calorimeter.

EEMC pre-shower layers, the shower maximum detector, the individual calorimeter

[1]SBIR (Small Business Innovation Research) is a highly competitive program within the Department of Energy that encourages small business to explore their technological potential and provides the incentive to profit from its commercialization.

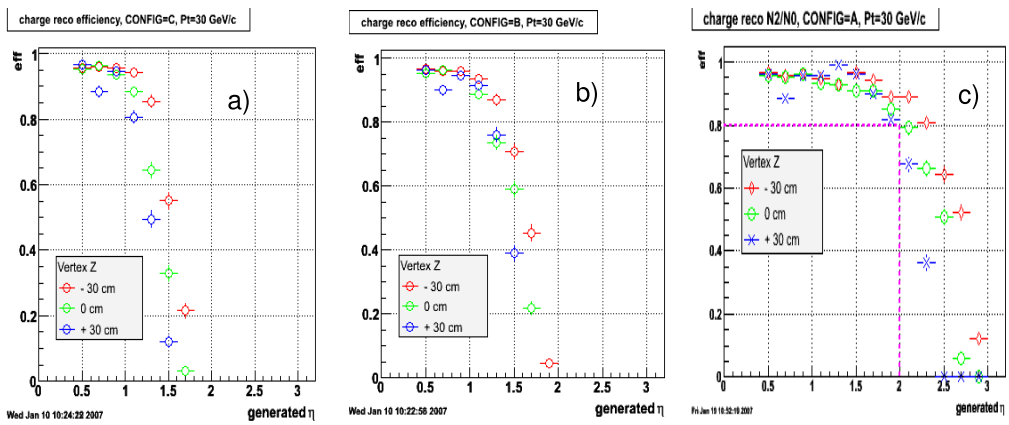

Figure 16: *Charge sign discrimination probability (ratio of the number of reconstructed tracks with correctly reconstructed charge sign divided by the number of generated tracks) for a) TPC + vertex only, b) TPC + vertex + EEMC SMD, c) all in b) plus FGT, SSD, and IST.*

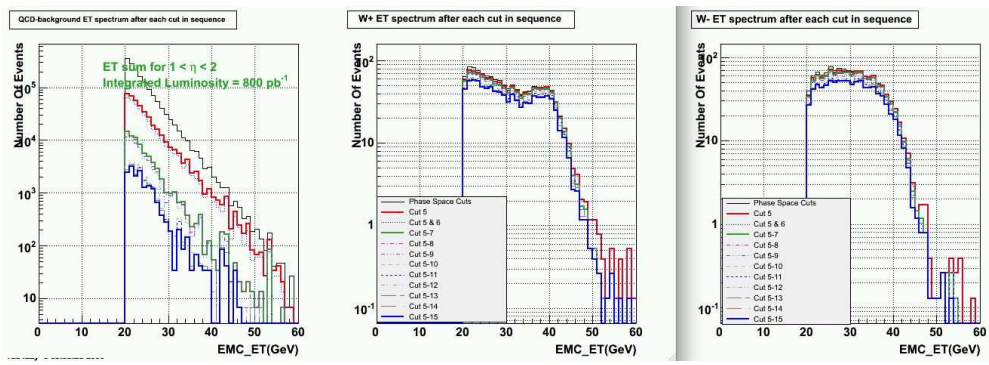

Figure 17: p_T *distribution for charged hadrons from a PYTHIA MC sample including detector effects in comparison to a PYTHIA MC sample of electrons from W events. A drastic reduction in background can be achieved while retaining most of the W signal events by requiring an isolation criteria and a missing* p_T *cut.*

towers and the post-shower layer are required to preserve suitable signal-to-background ratios at lower p_T where increasing hadronic background can dominate the electron/positron signal.

The EEMC subsystems are currently being used for the development of photon reconstruction algorithms. This effort will clearly benefit the required e/h discrimination for the W program in STAR.

The readout system for the proposed FGT is based on the APV25-S1 readout chip [49], which has been extensively tested for the CMS silicon tracker [50] and is also used for the COMPASS triple-GEM tracking detectors [51]. The same chip will also be used for the IST

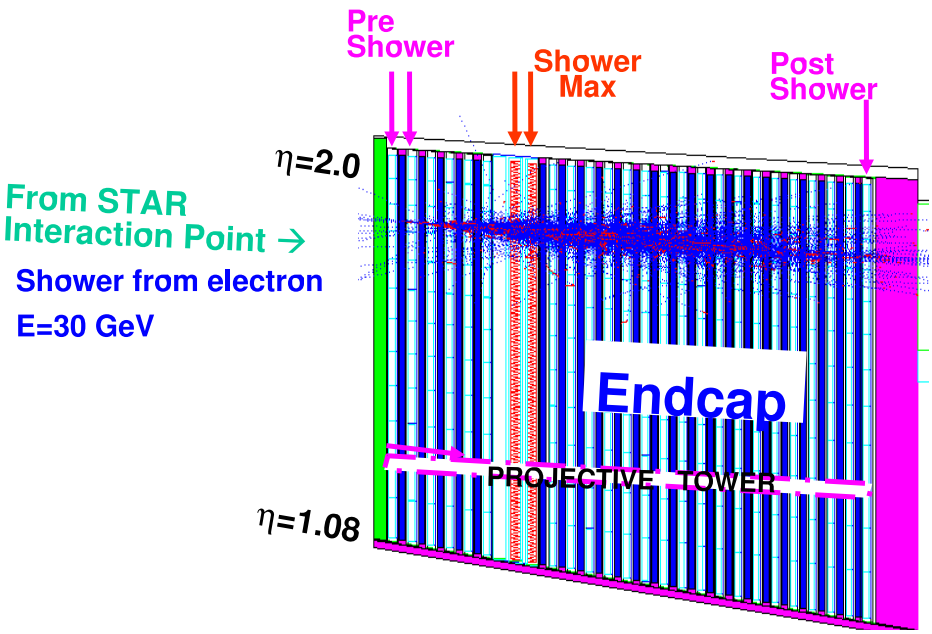

Figure 18: *Cross section of EEMC lower half. e/h discrimination will rely on measured longitudinal and transverse profile of the EM and hadronic showers. The plot shows a shower from a* 30 *GeV electron.*

in STAR. The use of a common chip readout system will significantly simplify the design of the overall readout system for the STAR tracking upgrade. The overall readout system is well developed.

The performance of a set of three triple-GEM prototype detectors has been evaluated during a testbeam experiment at FNAL in May 2007. Those prototype detectors are based on commercially produced GEM foils, a laser-etched 2D readout board along with a prototype APV25-S1 chip readout system and thus allowed to test the performance of the main components to be used for the actual FGT triple-GEM detectors. The results of the testbeam experiment clearly demonstrate that the requirements on the STAR forward tracking upgrade are met.

It should be stressed that the tracking upgrade for STAR, based on well-established, intrinsically fast detector and readout elements, will provide a significant improvement of the existing STAR tracking system, in particular for the expected high luminosity operation at RHIC.

The expected asymmetries in the forward and backward regions using the FGT after detector simulation of signal and background can be seen from Fig. 19 as a function of the lepton E_T and in Fig. 20 as a function of the lepton rapidity.

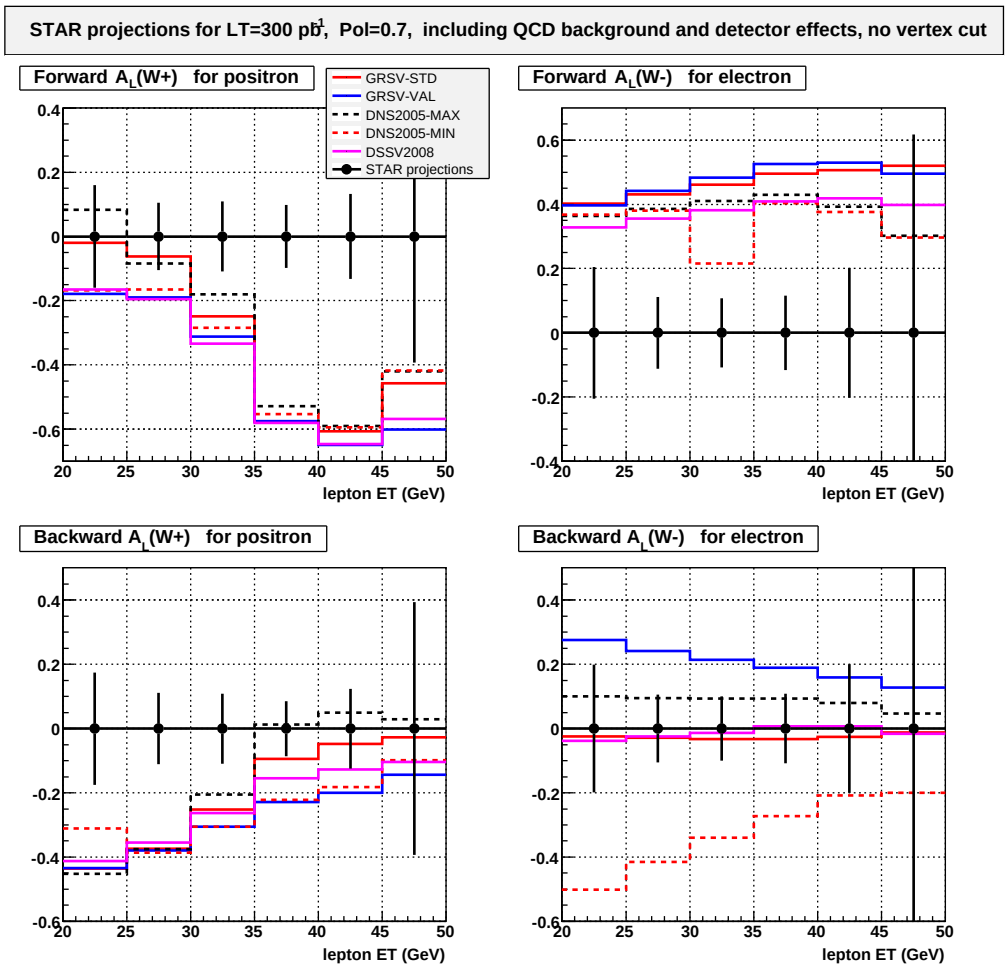

Figure 19: *Projected asymmetries in the forward/backward STAR region as a function of lepton E_T. The data has been obtained for GRSV standard, GRSV valence [31], DSSV [32], and DNS [20] using a maximal and minimal sea polarization scenario in RHICBOS [30] after detector simulation and inclusion of background for 300 pb^{-1} assuming 70% polarization.*

2.2 Central region

Figure 21 shows the projected uncertainties for $300\,\mathrm{pb}^{-1}$ and 70% beam polarization of A_L as a function of E_T in the mid-rapidity acceptance region of the STAR BEMC ($-1 < \eta < 1$). QCD background effects have not been included at this stage. Those are expected to be small. However, an electron finding efficiency of 70% has been taken into account similar to the STAR EEMC acceptance region of $1 < \eta < 2$. It is expected that the mid-rapidity region will provide additional important constraints on the polarized anti-quark distribution functions, in particular the polarized anti-d distribution function.

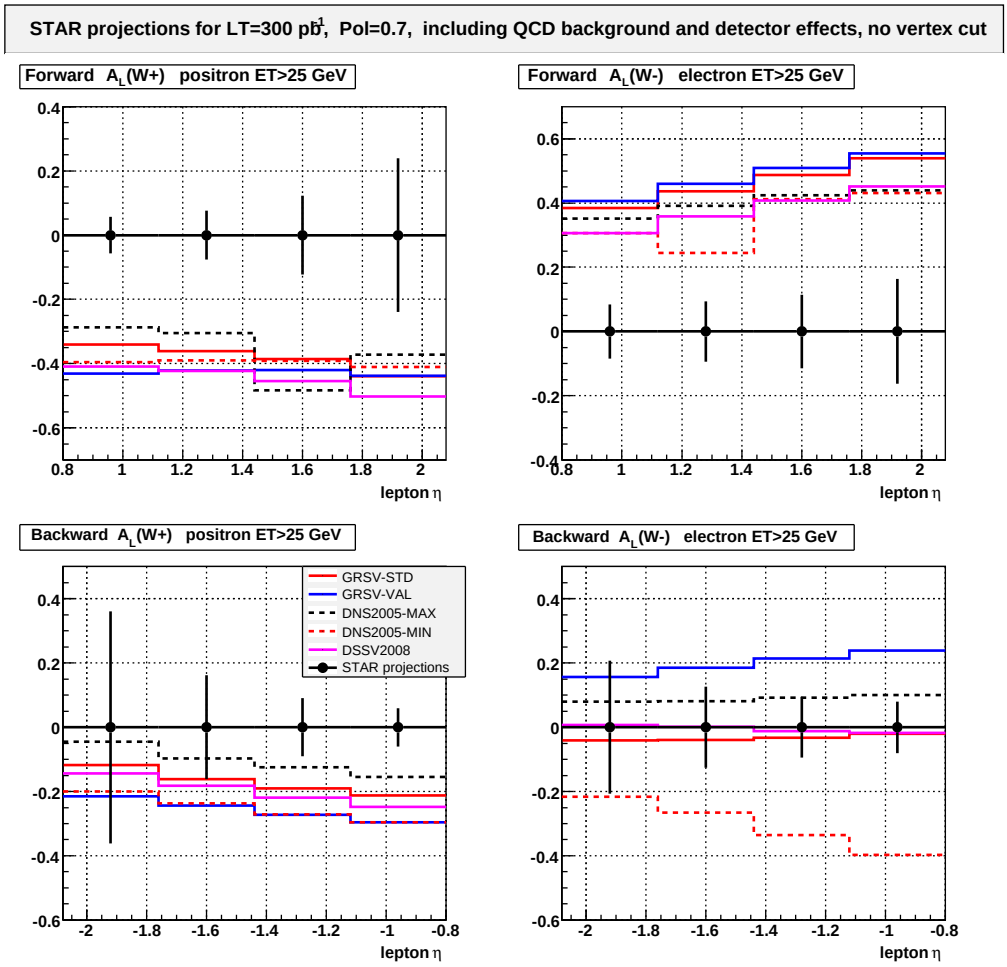

Figure 20: *Projected asymmetries in the forward/backward STAR region as a function of the lepton rapidity η. The data has been obtained for GRSV standard, GRSV valence [31], DSSV [32], and DNS [20] using a maximal and minimal sea polarization scenario in RHIC-BOS [30] after detector simulation and inclusion of background for 300 pb^{-1} assuming 70% polarization.*

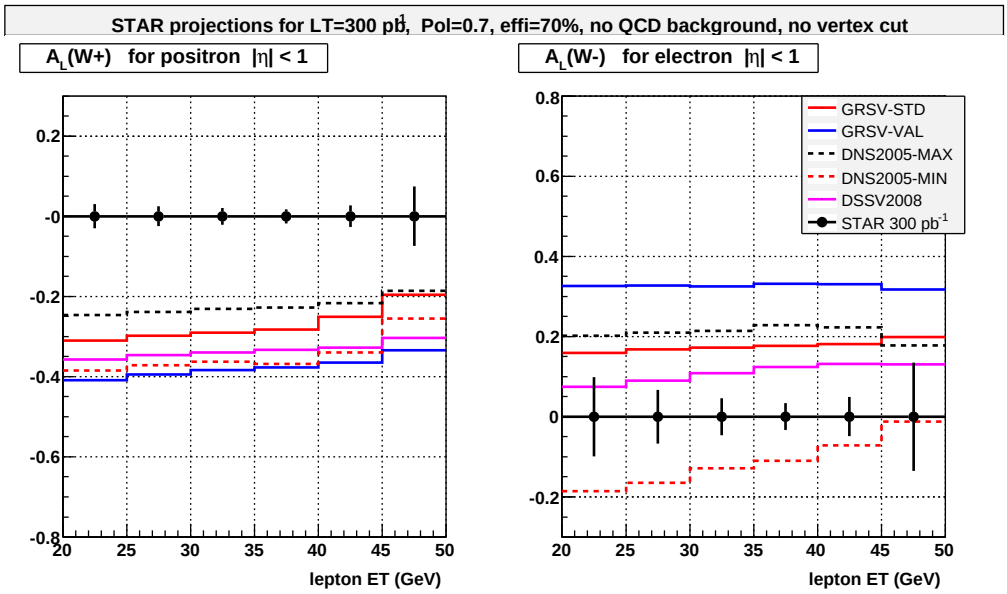

Figure 21: *Projected uncertainties for* $300\,pb^{-1}$ *and* 70% *beam polarization of* A_L *as a function of* E_T *in the mid-rapidity acceptance region of the STAR BEMC* ($-1 < \eta < 1$).

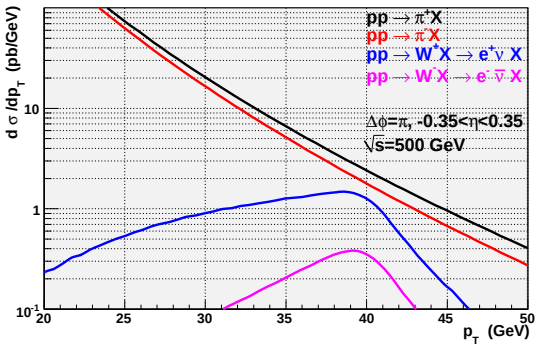

Figure 22: *Raw electron and positron yields in the central PHENIX detector from W decays (e^- purple, e^+ blue) and charged pion yields from other processes (π^+ black, π^- red).*

3 PHENIX W measurements

3.1 Central Arm electron asymmetries

The PHENIX central detectors provide good detection of W decays into electrons as a combination of the drift chambers and the electromagnetic calorimeter can separate them well from hadrons. As they will all be seen as high energy towers in the calorimeter the existing EMCAL trigger with a high threshold can be used.

The unpolarized W predictions come from RHICBOS [30], and use the CTEQ5M pdfs. The total cross section for $W^+ \to e^+\nu$ into the central arms is 21 pb and 3.5 pb for $W^- \to e^-\bar{\nu}$.

The charged pion background has been derived at NLO from the invariant cross sections using the CTEQ6M distribution function parameterization and DSS fragmentation functions at scale $\mu = p_T$ [52]. As can be seen in Fig. 22 the raw pion yields are dominating over the electrons from W decays at the same p_T, however no particle identification has been applied, yet.

Using the ratio of deposited energy in the EMCal over the obtained particle momentum one should be able to reject pions by at least a factor of 100 as they only deposit a small fraction of their energy in an electromagnetic calorimeter. Additionally, an electron isolation requirement (no jet activity around the electron in the central arm) should further reduce the pion background by a factor of 3 to 10. While no detailed simulation of these are available at present the combined rejection should make the W decay electrons in the PHENIX central detector a clean channel.

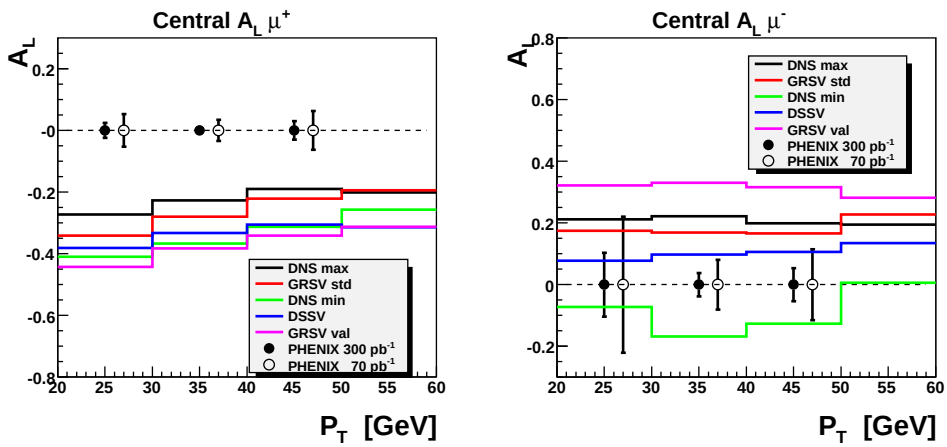

Figure 23: *Simulated asymmetries in the PHENIX central arms for $W^+ \to e^+\nu$ (left plot) and $W^- \to e^-\bar{\nu}$ as a function of p_T. The data has been obtained for GRSV standard, GRSV valence [31], DSSV [32], and DNS [20] using a maximal and minimal sea polarization scenario in RHICBOS [30] for 300 pb^{-1} (full symbols) and 70 pb^{-1} (open symbols) assuming 70% beam polarization.*

The remaining uncertainty of the electron decay channel lies in the correct momentum and charge reconstruction of a track. According to MC simulations of the PHENIX drift chambers the charge is reconstructed correctly 95% of the time, but the detector alignment has to be closely monitored to ensure this number. The momentum resolution is about 7 GeV for 40 GeV electrons which is acceptable.

The raw asymmetries as obtained from RHICBOS in the central arms of PHENIX are shown in Fig. 23 for the expected luminosities in the first full W running year(70 pb^{-1}), and for the planned W runnign through 2013 (300 pb^{-1}). It can be seen that in the central region quite sizable asymmetries can be observed. Even though the central region probes predominantly intermediate x one can still see differences in the two sea polarization scenarios. In particular the decay kinematics of the W^+ make the central region most sensitive to $\Delta\bar{d}$. Based on the raw asymmetries with a ideal detection this corresponds to a sensitivity to distinguish a maximal from a minimal DNS $\Delta\bar{d}$ on the level of 12 standard deviations with 300 pb^{-1}.

3.2 Muon arm asymmetries

The separation of spin dependent distributions for quarks and anti-quarks requires measurements in the forward/backward direction. In PHENIX this translates into measurements of $W \to \mu\nu$ using the muon spectrometer arms with an acceptance of $1.2 < |\eta| < 2.2$. The W-data sample will be defined as the sample of inclusive single muons with $p_T > 20$

GeV in the muon spectrometer downstream of an upstream hadron absorber. We have confirmed through detailed Monte Carlo simulations followed by a full reconstruction for large background samples and W-signal samples that the W-signal to background ratio in the inclusive single muon spectrum with $p_T > 25$ GeV will be S/B$\simeq$3:1 using the planned additional absorber [53]. The actual signal to background rate will be measured during run 9. As the background does not originate from parity violating decays it only dilutes the asymmetries but cannot introduce false ones.

We have found that the dominating background to the W-signal consists of decay muons from low momentum hadrons which first punch through the absorber upstream of the muon spectrometers and then decay in the volume of the muon spectrometer magnet such that the combination of upstream hadron track and downstream decay muon track is falsely reconstructed with high momentum. In order to reach a signal to background ratio of S/B=3:1 it will be necessary to insert two additional nuclear interaction lengths of absorber between the central magnet yoke and the upstream opening of the PHENIX muon spectrometers. The absorber can be integrated with the RPC upgrade and it is planned that the absorber be removable for heavy ion running if needed.

In addition to the absorber an upgrade of the first level muon trigger will be required to be able to reduce the raw proton-proton collision rates of up to 8 MHz to the available bandwidth of the PHENIX data acquisition systems. The muon trigger upgrade encompasses two components: a new dedicated muon trigger spectrometer based on RPC technology and new front-end electronics for the PHENIX muon tracking chambers which will pass information from the muon tracking chamber front end to the first level trigger processors.

In the trigger the muon tracker and RPC information will be complementary: the muon tracker will provide precise tracking information and allow for a tighter momentum cut. The RPCs have better timing resolution and will be used not only for the momentum measurement but also for the rejection of beam related backgrounds in the trigger and the suppression of cosmic rays in the offline analysis. The timing information also will be used to correctly align W-event information with the beam polarization information.

The muon tracker front-end trigger electronics has been developed by a team of Japanese collaborators in PHENIX under the leadership of groups at KEK and Kyoto University and with the support of a $2.6M grant from the Japanese Society for the Promotion of Science. The muon tracker trigger electronics technical design report has been reviewed at BNL on November 29, 2007. It is currently planned to carry out the installation of the electronics during the summer shutdowns of 2008 (all north muon spectrometers tracker stations 1, 2 and 3) and 2009 (all south muon spectrometer tracker stations 1, 2 and 3). It will contribute one part of the muon trigger.

The RPC muon trigger detector will be based on technology which has been developed

at Korea University in Seoul for the CMS forward muon trigger bakelite RPCs at the LHC. CMS forward trigger RPCs stand out in reaching an aerial rate capability in excess of 2 kHz/cm^2 at low cost and a timing resolution of about 2ns. In contrast, glass RPC technology reaches far better timing resolution but is limited to rates of typically below 50 Hz/cm^2 and is far too expensive to cover the 180 m^2 area needed in the PHENIX muon trigger upgrade.

The RPC upgrade is supported through a $2M NSF major research equipment initiative under the leadership of the University of Illinois and $0.3M of institutional contributions from Iowa State University, University of California at Riverside, University of Illinois and the RIKEN BNL Research Center. Overall the muon trigger upgrade project presently involves 83 physicists and students from 19 institutions in PHENIX. RPC mass production is anticipated to start in the summer of 2008 and the installation will occur in increments during the summer months in 2009 (RPC stations 2 and 3 and Absorber North), 2010 (RPC stations 2 and 3 and Absorber South) and 2011 (RPC stations 1 North and South if needed). Therefore a first full trigger consisting of the FEEs and two Planes of RPCs will be available for one side in 2009 and for both sides in 2010.

3.2.1 Trigger performance

In order to develop and refine the design of the muon forward trigger a set of Monte Carlo simulations were performed. These simulations relied on the full PHENIX detector simulation package PISA, and simulated events were generated using the full PHENIX detector geometry expected to be in place during the time period when the muon forward trigger is expected to be running. The goal of these simulations is to demonstrate sufficient rejection power and redundancy in the trigger design to achieve the physics goals of the polarized proton program.

The forward muon trigger algorithm is RPC-driven, and works by making combinations of RPC1-2 hits and then using projections of this combination to establish confirming hits in RPC3 and MuTr Station 2. The full detector granularity of the RPC stations is not used in the LVL1 trigger. Instead, rings of identical strip width will be combined at LVL1 to form four regions in theta over the full acceptance, as opposed to the nominal eight regions. Of the two stations at RPC1, it is assumed that only RPC1a is instrumented for the trigger. In the trigger simulations, hit matching is done within windows in theta angle at the RPC chambers. Practically, this will correspond to a hardware mapping between channels in the different RPC detectors.

The efficiency of the trigger algorithm was checked using simulated 25 GeV/c single muon tracks. The efficiencies for single muon tracks vary between 92-98% as a function of the ϕ angle cut between the RPC1 and RPC2 hits. An angle cut of 3 degrees is chosen to

Table 1: *Trigger rejections for pp minbias events at = 500 GeV. A nominal RPC noise rate of 10 Hz/cm^2 was included in the simulations.*

	North Arm	South Arm	Combined
$\phi \leq 2$ degrees	76,700	23,200	17,800
$\phi \leq 3$ degrees	47,500	15,600	11,800

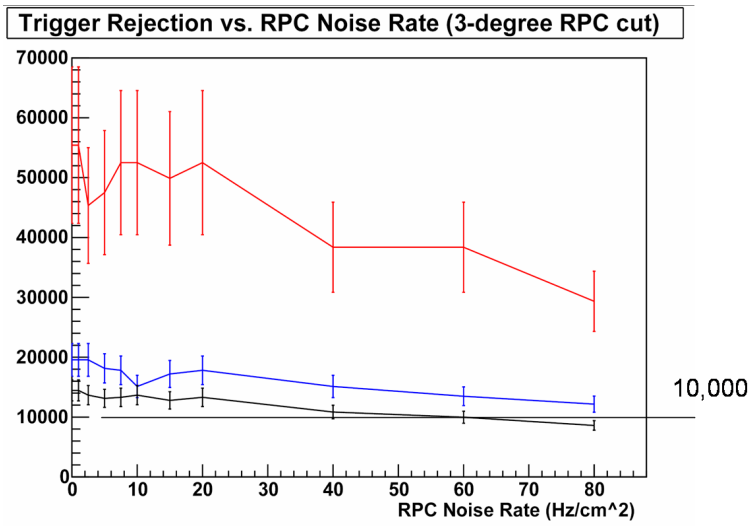

Figure 24: *Forward muon trigger rejection versus RPC noise rate. The error bars shown are the statistical errors on the rejection factors.*

maintain high efficiency for high-momentum single muon tracks. In the tables that follow we will quote rejection power for both the three degree and two degree RPC angle cuts, with the understanding that additional rejection power can be obtained by a small sacrifice of efficiency for high momentum muons.

The expected rejection of the muon forward trigger is listed in Table 1. A nominal RPC noise rate of 10 Hz/cm^2 was assumed in these simulations. The combined north and south arm rejections allow all real events to be recorded, given the DAQ bandwidth, without need to scale down.

Finally, we examined the stability of the trigger rejection vs. the noise rate of the RPC chambers. The results are shown in Fig. 24. The trigger rejection factor for the combined arms remains above 10,000 for RPC noise rates < 50 Hz/cm^2.

3.2.2 MC Simulation and Analysis of the W Physics Program

There is great interest in measuring the spin contribution of light (anti)quarks in the proton via the production of W bosons ($u + \bar{d} \rightarrow W^+$ and $d + \bar{u} \rightarrow W^-$). The rate for W production in proton-proton collisions at 500 GeV is small and thus the measurement requires high luminosity running and a high signal to background ratio. In order to interpret the measured muon asymmetry in terms of flavor separated polarized quark distributions, it is important for the PHENIX muon spectrometers to measure both the muon charge sign as well as its p_T. In addition there are multiple possible sources of background for high p_T muon candidates to the $W \rightarrow$ muon measurement. Those are:

1. High p_T muons from heavy flavor (D and B) semi-leptonic decays. However, earlier studies indicate the p_T distribution even for bottom quarks falls off and have contributions well below the W $\rightarrow$ muons at $p_T > 20$ GeV/c.
2. Some light hadrons (pions and kaons) will decay into muons before the front absorber and then penetrate the muon spectrometer as muons. These contributions are included in our simulation. However, the p_T distribution for these light hadrons falls steeply and thus mostly contributes at low p_T .
3. Decay muons, which undergo a large scattering interaction in MuTr station 2 and thus have a mis-reconstructed high p_T. We find that this contribution is small, noting that station 2 has little material.
4. High p_T light hadrons can punch through the absorber and into the MuID. These reconstruct near the correct p_T, but their cross sections are small.
5. Light hadrons can punch through the absorber, and then decay into muons inside the MuTr tracking volume. The kink angle from the decay can lead to an incorrect determination of the reconstructed p_T, and thus low p_T hadrons can create fake high p_T background.

For backgrounds 1-3 we find negligible contributions at high p_T and that the rate for background 4 becomes lower than the $W \rightarrow$ muon rate above a $p_T > 20$ GeV. The fake high p_T tracks, type 5, are the dominant source of background and lead to a predicted signal/background of 1/3 with the current detector included and 3/1 with an additional absorber.

In Figure 25, we plot the breakdown of the initial background contributions by the originating light hadron type. We plot the combined π^+ and π^- contribution as Pions and then the different charge sign kaons separately. This background is larger for kaons than for pions due to the shorter lifetime ($c\tau_{kaon} = 3.7$ m, $c\tau_{pion} = 7.8$ m) and also the smaller Lorentz boost for the kaon at the same p_T. The W signal is shown for both charges

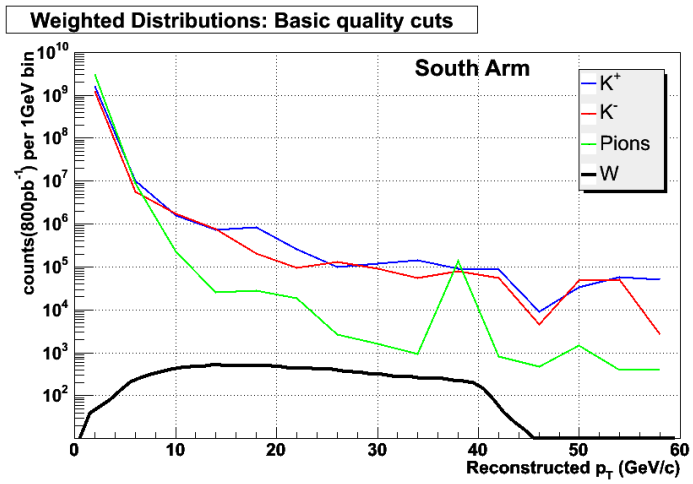

Figure 25: *Raw false high p_T background from kaon and pion decay yields vs the W-signal without absorber and tight track quality cuts.*

together, but the yields are only approximate as here only a PYTHIA simulation was used as input to the detector simulation which is known to underestimate the yields. However the raw background level is three orders of magnitude higher than the signal. Note that the background distribution continues smoothly above $p_T > 40$ GeV/c, but the W $\rightarrow$ muon signal does not. However, for reconstructed W decay muons detector resolution will also smoothen the kinematic edge of the p_T distribution.

As an addition to this analysis the effect of possible absorbers was tested which reduces the background by another order of magnitude. Since the contribution of kaons at low transverse momenta are dominating the background only K^+ with transverse momenta between 1-2 and 2-3 GeV were created (while K^- are similar). The momentum distributions after applying the basic cuts rescaled for a 800 pb^{-1} data sample are shown in Figure 26. It can be clearly seen that each additional level of absorbers reduces the amount of background significantly. With a tighter set of track quality cuts which are found to be 95% efficient for W decay muons one can obtain additional rejection power of more than a factor 100. Higher rejection factors are possible but could not be tested so far due to the limited amont of remaining partcles in the simulation.

3.2.3 Tracking in p + p Collisions at High p_T

The general tracking of the high momentum muons from W decays will be performed with the already existing MuTr detector. The limited position resolution of the MuTr will have an effect on the momentum resolution of the reconstructed muons. For this purpose MC studies have been performed. At high momenta the large tail to higher momenta

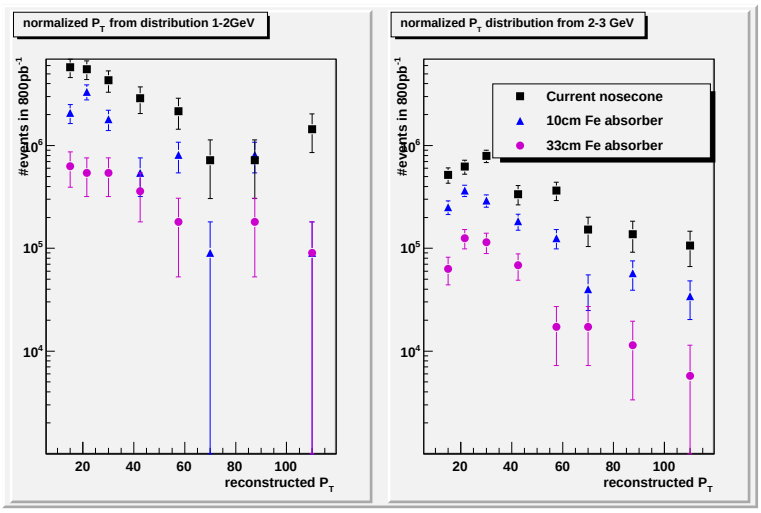

Figure 26: *Lowenergetic K^- background falsely reconstructed at high p_T in the muon spectrometer depending on the thickness of the hadron absorber.*

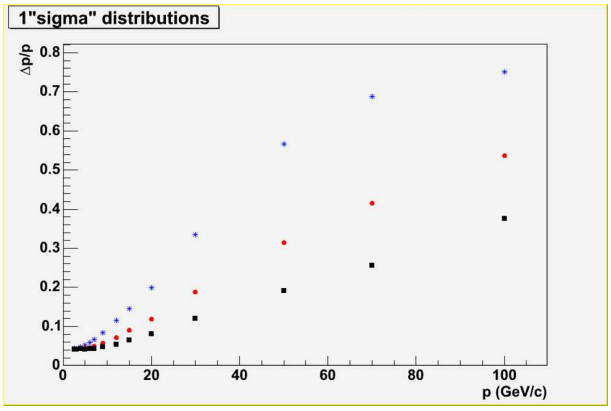

Figure 27: *Momentum resolution for three different position resolutions in the muon tracker: 600 μm (blue), 300 μm (red) and 150 μm (black).*

dominates these resolutions as can be seen in Fig. 27. This tail to higher momenta is due to the very small angular deviation of such a track in the magnetic field. The finite resolution of the MuTr might even lead to a misidentification of the charge sign of the muon which could have severe implications on the extraction of the quark and sea quark (helicity) distributions. The fraction of muons with misidentified charge reaches less than 3% at highest momenta when assuming a position resolution of 300 μm for the momentum range of muons originating from W decays. In the W analysis these misidentified fractions have to be corrected for, but correspond to a minor change in the reconstructed asymmetries.

3.2.4 W Production Modeling

The W signal was generated using the NLO Q_T resummed generator RHICBOS [30]. It estimates the cross sections for W^+ and W^- from proton-proton reactions at 500 GeV for the two muon arms, $1.2 < |\eta| < 2.2$, as 21.8 pb and 15.0 pb respectively. For 300 (1300) pb^{-1} of integrated RHIC luminosity, 2900 (11700) W^+ and 3200 (12800) W^- are expected in the muon arms for $p_T > 20$ GeV/c. The roughly equal numbers are due to the different production levels being canceled by the different kinematic distribution of the Ws. The reconstructed numbers with the full detector simulation are on the order of 2300 (10,000) events each.

The different helicity cross sections were generated using polarized distribution functions in RHICBOS based on DNS maximal and minimal sea scenarios [20], GRSV-2000 standard (red) and valence (blue) [54] and DSSV [32]. One can see the effect of the polarized quark distributions already in the very different yields for positive and negative helicity states which then translates into large asymmetries. The Jacobian peak disappears in the reconstructed cross sections due to momentum resolution. However, this does not affect the reconstruction of large asymmetries.

For the asymmetry reconstruction the events generated by RHICBOS were fed into the standard PHENIX detector simulation based on GEANT3 including dead channels of the muon detectors. Based on the previously described studies on the background rates an overall signal to background ratio of 3/1 was implemented in the asymmetry calculation and the tight cuts were applied. A polarization of 70% was assumed. The asymmetries for forward, backward $\mu^\pm$ for the different polarized parameterizations are shown as a function of the reconstructed p_T in the acceptance after applying tight cuts and after inclusion of a 3/1 signal to background ratio can be seen in Fig 28.

One clearly sees very large parity-violating asymmetries which reach about 30% for forward μ^+ and almost 50% for forward μ^-. The overall measurements in the forward direction will be significantly nonzero on the order of more than 6 standard deviations with a luminosity of about 70 pb^{-1} for W^- and about 3 standard deviations for W^+. In addition, it is also possible to distinguish different polarized parameterizations. While all parameterizations roughly agree on the quark polarizations the sea polarizations are very different. The differences between the polarized sea scenarios are becoming even more evident in the backward region where one is most sensitive to the $\Delta\bar{u}$ polarization in the μ^- channel. Here one can reach a sensitivity to distinguish between a maximal and a minimal DNS $\Delta\bar{u}$ on the 12 σ level with 300 pb^{-1}. Due to only detecting the decay muon the sensitivity to the $\Delta\bar{d}$ polarization in the μ^+ channel is higher at central rapidities.

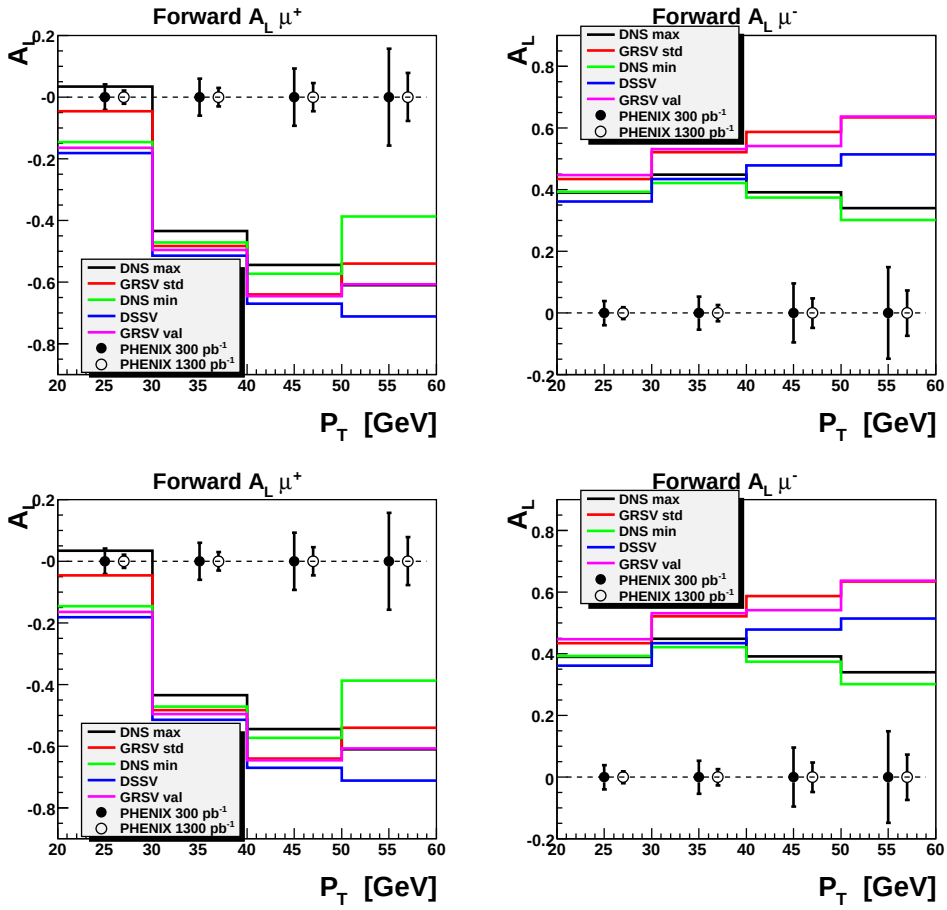

Figure 28: *Longitudinal single spin asymmetries for μ^+ and μ^- in the forward (top plots) and backward (bottom plots) regions of the PHENIX detector as a function of the reconstructed muon p_T. The data has been obtained for GRSV standard, GRSV valence [31], DSSV [32], and DNS [20] using a maximal and minimal sea polarization scenario in RHICBOS [30] after detector simulation and inclusion of background for 319 pb^{-1} (full symbols) and 1300 pb^{-1} (open symbols) assuming 70% beam polarization.*

3.2.5 Impact of other detector upgrades:

In addition to the already mentioned upgrades two further detector upgrades in PHENIX will further improve the W sensitivity by reducing the amount of background. The Forward vertex detector, FVTX and the nose cone calorimeter, NCC will be installed upstream of the central magnet yoke while the muon trigger RPCs and the additional hadron absorber will be installed downstream of the central magnet yoke. Both the FVTX and NCC promise significant additional rejection of the background through isolation cuts, precision track and vertex matching or cuts on energy loss.

References

[1] G. Bunce, N. Saito, J. Soffer, and W. Vogelsang, Ann. Rev. Nucl. Part. Sci. **50**, 525 (2000), hep-ph/0007218.

[2] RHIC SPIN collaboration, G. Bunce et al., BNL internal document, Status and Prospects of the RHIC Spin Physics Program.

[3] European Muon, J. Ashman *et al.*, Phys. Lett. **B206**, 364 (1988).

[4] European Muon, J. Ashman *et al.*, Nucl. Phys. **B328**, 1 (1989).

[5] Spin Muon, B. Adeva *et al.*, Phys. Rev. **D58**, 112002 (1998).

[6] E142, P. L. Anthony *et al.*, Phys. Rev. **D54**, 6620 (1996), hep-ex/9610007.

[7] E143, K. Abe *et al.*, Phys. Rev. **D58**, 112003 (1998), hep-ph/9802357.

[8] E154, K. Abe *et al.*, Phys. Rev. Lett. **79**, 26 (1997), hep-ex/9705012.

[9] E155, P. L. Anthony *et al.*, Phys. Lett. **B463**, 339 (1999), hep-ex/9904002.

[10] OPAL, K. Ackerstaff *et al.*, Phys. Lett. **B404**, 213 (1997), hep-ex/9707023.

[11] HERMES, A. Airapetian *et al.*, Phys. Lett. **B442**, 484 (1998), hep-ex/9807015.

[12] E. W. Hughes and R. Voss, Ann. Rev. Nucl. Part. Sci. **49**, 303 (1999).

[13] M. Anselmino, A. Efremov, and E. Leader, Phys. Rept. **261**, 1 (1995), hep-ph/9501369.

[14] H.-Y. Cheng, Int. J. Mod. Phys. **A11**, 5109 (1996), hep-ph/9607254.

[15] B. Lampe and E. Reya, Phys. Rept. **332**, 1 (2000), hep-ph/9810270.

[16] S. D. Bass, Eur. Phys. J. **A5**, 17 (1999), hep-ph/9902280.

[17] Spin Muon, B. Adeva *et al.*, Phys. Lett. **B420**, 180 (1998), hep-ex/9711008.

[18] HERMES, K. Ackerstaff *et al.*, Phys. Lett. **B464**, 123 (1999), hep-ex/9906035.

[19] X.-d. Jiang, P. E. Bosted, M. Jones, and D. Day, (2004), hep-ex/0412010.

[20] D. de Florian, G. A. Navarro, and R. Sassot, Phys. Rev. **D71**, 094018 (2005), hep-ph/0504155.

[21] S. Kretzer, Phys. Rev. **D62**, 054001 (2000), hep-ph/0003177.

[22] B. A. Kniehl, G. Kramer, and B. Potter, Nucl. Phys. **B582**, 514 (2000), hep-ph/0010289.

[23] N. S. Craigie, K. Hidaka, M. Jacob, and F. M. Renard, Phys. Rept. **99**, 69 (1983).

[24] C. Bourrely, J. Soffer, and E. Leader, Phys. Rept. **59**, 95 (1980).

[25] C. Bourrely and J. Soffer, Phys. Lett. **B314**, 132 (1993).

[26] C. Bourrely and J. Soffer, Nucl. Phys. **B423**, 329 (1994), hep-ph/9405250.

[27] P. Chiappetta and J. Soffer, Phys. Lett. **B152**, 126 (1985).

[28] C. Bourrely and J. Soffer, Nucl. Phys. **B445**, 341 (1995), hep-ph/9502261.

[29] B. Kamal, Phys. Rev. **D57**, 6663 (1998), hep-ph/9710374.

[30] P. M. Nadolsky and C. P. Yuan, Nucl. Phys. **B666**, 31 (2003), hep-ph/0304002.

[31] M. Gluck, E. Reya, M. Stratmann, and W. Vogelsang, Phys. Rev. **D63**, 094005 (2001), hep-ph/0011215.

[32] D. de Florian, R. Sassot, M. Stratmann, and W. Vogelsang, (2008), 0804.0422.

[33] T. Gehrmann, Nucl. Phys. **B534**, 21 (1998), hep-ph/9710508.

[34] New Muon, P. Amaudruz *et al.*, Phys. Rev. Lett. **66**, 2712 (1991).

[35] New Muon, M. Arneodo *et al.*, Phys. Rev. **D50**, 1 (1994).

[36] NA51, A. Baldit *et al.*, Phys. Lett. **B332**, 244 (1994).

[37] FNAL E866/NuSea, E. A. Hawker *et al.*, Phys. Rev. Lett. **80**, 3715 (1998), hep-ex/9803011.

[38] HERMES, K. Ackerstaff *et al.*, Phys. Rev. Lett. **81**, 5519 (1998), hep-ex/9807013.

[39] B. Dressler *et al.*, Eur. Phys. J. **C18**, 719 (2001), hep-ph/9910464.

[40] B. Dressler, K. Goeke, M. V. Polyakov, and C. Weiss, Eur. Phys. J. **C14**, 147 (2000), hep-ph/9909541.

[41] T. Gehrmann and W. J. Stirling, Phys. Rev. **D53**, 6100 (1996), hep-ph/9512406.

[42] Asymmetry Analysis, M. Hirai, S. Kumano, and N. Saito, Phys. Rev. **D69**, 054021 (2004), hep-ph/0312112.

[43] STAR, L. C. Bland, RIKEN Rev. **28**, 8 (2000), hep-ex/0002061.

[44] P. Nadolsky, Rhicbos, 2007, Invited talk at the RIKEN BNL Research Center Workshop on Parity-Violating Spin Asymmetries at RHIC.

[45] H. Avakian, S. J. Brodsky, A. Deur, and F. Yuan, Phys. Rev. Lett. **99**, 082001 (2007), 0705.1553.

[46] S. Vidgor, The rhic spin program: Snapshots of progress, 1998, hep-ex/9905034, Invited talk at the 13th International Symposium on High-Energy Spin Physics (SPIN98).

[47] S. B. I. Research, US-DOE SBIR grant DE-FG02-05ER84169, http://sbir.er.doe.gov/sbir/.

[48] B. Surrow *et al.*, Nucl. Instrum. Meth. **A572**, 201 (2007).

[49] M. J. French *et al.*, Nucl. Instrum. Meth. **A466**, 359 (2001).

[50] CMS, CERN-LHCC-98-06.

[51] M. C. Altunbas *et al.*, Nucl. Instrum. Meth. **A490**, 177 (2002).

[52] Werner Vogelsang, private communication.

[53] The PHENIX forward moun upgrade group, BNL internal document, https://www.phenix.bnl.gov/WWW/p/draft/jhill/DOE_Oct15, Measurement of the Parity Violating Spin Asymmetries with the PHENIX Detector at RHIC.

[54] M. Gluck, E. Reya, M. Stratmann, and W. Vogelsang, Phys. Rev. **D53**, 4775 (1996), hep-ph/9508347.

[55] J. I. Friedman and H. W. Kendall, Annu. Rev. Nucl. Sci. 22 (1972) 203.

[56] H. Abromowicz et al., Z. Phys. C15 (1982) 19.

[57] J. M. Conrad, M. H. Shaevitz and T. Bolton, Rev. Mod. Phys. 70 (1998) 1341.

[58] K. Gottfried, Phys. Rev. Lett. 18 (1967) 1174.

[59] E. D. Bloom et al., Proc. 15th Int. Conf. on High Energy Phys., Kiev, USSR (1970).

[60] E. D. Bloom, Proc. 6th Int. Sym. on Electron and Photon Interactions at High Energies, edited by H. Rollnik and W. Pfeil (North-Hollan, Amsterdam, 1974) 227.

[61] J. J. Aubert et al., Nucl. Phys. B293 (1987) 740.

[62] M. Arneodo et al., Phys. Rev. D50 (1994) R1.

[63] A. Baldit et al., Phys. Lett. B342 (1995) 339

[64] R. S. Towell et al., Phys. Rev. D64 (2001) 052002

[65] K. Ackerstaff et al., Phys. Rev. Lett. 81 (1998) 5519

[66] S. Kumano, Phys. Rep. 303 (1998) 5519

[67] J. Speth, and A. W. Thomas, Adv. Nucl. Phys. 24 (1998)83

[68] G. T. Garvey and J. C. Peng, Prog. Part. Nucl. Phys., 47 (2001) 203

[69] V. D. Barger and R. J. N. Phillips, Collider Physics (Addison - Wesley Publishing Company, 1987).

[70] J. Alitti et al., Phys. Lett. B276 (1992) 365.

[71] F. Abe et al., Phys. Rev. D44 (1991) 29; W. F. Badgett, Fermilab Preprint, FERMILAB-Conf-94/258-E(1994).

[72] F. Abe et al., Phys. Rev. Lett. 68 (1992) 1458.J. Alitti et al., Phys. Lett. B276 (1992) 365.

[73] J. C. Peng and D. M. Jansen, Phys. Lett. B354 (1995) 460

[74] D. Acosta et al.,Phys. Rev. D71, (2005) 051104.